2016-06-15

From ether to acid: a plausible degradation pathway of glycerol dialkyl glycerol tetraethers

Liu, X-L

10.1016/j.gca.2016.04.016
Geochimica et Cosmochimica Acta

From ether to acid: a plausible degradation pathway of glycerol dialkyl glycerol tetraethers

Xiao-Lei Liu [a, b, *], Daniel Birgel [c], Felix J. Elling [a, ♯], Paul A. Sutton [d], Julius S. Lipp [a], Rong Zhu [a, §], Chuanlun Zhang [e], Martin Könneke [a], Jörn Peckmann [c, f], Steven J. Rowland [d], Roger E. Summons [b], Kai-Uwe Hinrichs [a]

[a] Organic Geochemistry Group, MARUM Center for Marine Environmental Sciences and Department of Geosciences, University of Bremen, 28359 Bremen, Germany

[b] Department of Earth, Atmospheric, and Planetary Sciences, Massachusetts Institute of Technology, 77 Massachusetts Avenue, Cambridge, MA 02139-4307, USA

[c] Institute of Geology, University of Hamburg, 20146 Hamburg, Germany

[d] School of Geography, Earth and Environmental Sciences, University of Plymouth, Plymouth, Devon PL4 8AA, U.K.

[e] State Key Laboratory of Marine Geology, Tongji University, Shanghai 200092, China

[f] Department of Geodynamics and Sedimentology, Center for Earth Sciences, University of Vienna, 1090 Vienna, Austria

[♯] Present address, Harvard University, 20 Oxford St, Cambridge, MA 02138, USA

[§] Present address, ETH Zurich, Universitätsstrasse 16, 8092 Zürich, Switzerland

* Corresponding author, E-mail: xlliu@mit.edu

Abstract

Glycerol dialkyl glycerol tetraethers (GDGTs) are ubiquitous microbial lipids with extensive demonstrated and potential roles as paleoenvironmental proxies. Despite the great attention they receive, comparatively little is known regarding their diagenetic fate. Putative degradation products of GDGTs, identified as hydroxyl and carboxyl derivatives, were detected in lipid extracts of marine sediment, seep carbonate, hot spring sediment and cells of the marine thaumarchaeon *Nitrosopumilus maritimus*. The distribution of GDGT degradation products in environmental samples suggests that both biotic and abiotic processes act as sinks for GDGTs. More than a hundred newly recognized degradation products afford a view of the stepwise degradation of GDGT via 1) ether bond hydrolysis yielding hydroxyl isoprenoids, namely, GDGTol (glycerol dialkyl glycerol triether alcohol), GMGD (glycerol monobiphytanyl glycerol diether), GDD (glycerol dibiphytanol diether), GMM (glycerol monobiphytanol monoether) and bpdiol (biphytanic diol); 2) oxidation of isoprenoidal alcohols into corresponding carboxyl derivatives and 3) chain shortening to yield C_{39} and smaller isoprenoids. This plausible GDGT degradation pathway from glycerol ethers to isoprenoidal fatty acids provides the link to commonly detected head-to-head linked long chain isoprenoidal hydrocarbons in petroleum and sediment samples. The problematic C_{80} to C_{82} tetraacids that cause naphthenate deposits in some oil production facilities can be generated from H-shaped glycerol monoalkyl glycerol tetraethers (GMGTs) following the same process, as indicated by the distribution of related derivatives in hydrothermally influenced sediments.

1. INTRODUCTION

Lipid biomarkers have the potential of providing valuable information regarding the composition of ancient ecosystems and paleoenvironmental conditions throughout most of the sedimentary record (e.g., Peters et al., 2004). For most of the frequently used biomarkers, such as steroids, hopanoids, pigments and their derivatives, the post-depositional structural transformations are rather well constrained (e.g., Mackenzie et al., 1982; Innes et al., 1997; Peters et al., 2004; Brocks and Schaeffer, 2008) and contribute to the foundation of the geological biomarker concept that links geomolecules to their biological precursors. An exception is the intensively studied group of isoprenoidal glycerol dialkyl glycerol tetraether (GDGT) lipids produced by Archaea. Despite their prominent use as molecular proxies for the reconstruction of paleoenvironmental conditions (e.g., Pearson and Ingalls, 2013; Schouten et al., 2013) and, in their intact polar form, for the ecology of extant archaeal communities (e.g., Lipp and Hinrichs, 2009; Liu et al., 2011; Meador et al., 2015; Yoshinaga et al., 2015), our understanding of their post-depositional behavior is fragmentary.

Three principal archaeal lipid categories are observed in environmental and geological samples: (i) intact polar lipids (IPL) as building blocks of the cellular membrane, consisting of a glycerolalkylether backbone and a polar headgroup which, in most instances, is glycosidic (Sturt et al., 2004, Lipp and Hinrichs, 2009), (ii) the corresponding core glycerol alkyl ethers derived from hydrolytic cleavage of the polar headgroups on timescales of days to several tens of millennia, depending on depositional

conditions and enzymatic activity (Harvey et al., 1986; Xie et al., 2013), and (iii) degradation products of core glycerol alkyl ethers that occur as hydrocarbons (Moldowan and Seifert, 1979), alcohols (Schouten et al., 1998; Saito and Suzuki, 2010) and carboxylic acids (Meunier-Christmann, 1988; Schouten et al., 2003; Birgel et al., 2008a).

The second group, i.e., the core lipids, is among the most extensively studied biomarker class in the last decade (Pearson and Ingalls, 2013; Schouten et al., 2013), in particular the GDGT derivatives. More than thirty yeas ago Chappe et al. (1982) had reported the widespread presence of glycerol di- and tetraethers in sediments and petroleum. GDGTs accumulate in cold and moderately heated aquatic sediments with seemingly little molecular alteration and remain intact in sediments over tens of millions of years (e.g., Kuypers et al., 2001). GDGTs, including the bacterial non-isoprenoidal types (Weijers et al., 2006; Liu et al., 2012b), are among the most prominent lipids in marine sediments and soils. Their ubiquity and abundance result from both the widespread distribution of their producing, largely uncultured, microbes and their relatively high recalcitrance caused by the ether-linkages. Within the domain Archaea, GDGTs are taxonomically widely distributed and probably produced by members of all phyla (Pearson and Ingalls, 2013; Schouten et al., 2013).

Thermal diagenesis (Rowland, 1990) and hydrous pyrolysis (Pease et al., 1998) experiments have shown the generation of isoprenoidal hydrocarbons from fresh archaeal cultures. The exact fate of GDGTs is not clear, but they seem to be the most plausible precursors of a wealth of compounds of putative archaeal origin found in thermally

95 mature formations. These compounds include head-to-head linked C_{32} to C_{40} isoprenoid
96 hydrocarbons in petroleum samples (Moldowan and Seifert, 1979), biphytanic diols
97 (Schouten et al., 1998; Saito and Suzuki, 2010) and biphytanic diacids (Meunier-
98 Christmann, 1988; Birgel et al., 2008a) in recent sediments and rock samples of possibly
99 diagenetic and/or biogenic origin; however these diols or diacids have never been
100 detected in any archaeal cell extracts. Another group of recently discovered, widespread
101 compounds includes a series of glycerol ether derivatives, the glycerol dibiphytanol
102 diethers (GDDs; Knappy and Keely, 2012; Liu et al., 2012a). Although the occurrence of
103 core GDDs and their glycosidic intact polar lipids in archaeal cell extracts suggests that
104 they play a role in archaeal lipid biosynthesis (Liu et al., 2012a; Meador et al., 2014), a
105 diagenetic contribution of these lipids in natural settings cannot be ruled out (e.g., Yang
106 et al., 2014).
107
108 Another conspicuous compound series of putative archaeal origin are the so-called 'H-
109 shaped' or 'ARN' C_{80}-C_{82} isoprenoidal tetracarboxylic acids found in certain petroleum
110 types (Lutnaes et al., 2006, 2007) and believed to contribute significantly to the
111 problematic naphthenate deposits formed during oil processing (e.g., Baugh et al., 2004;
112 2005). The archaeal lipids that are structurally related to the C_{80} tetraacids are 'H-shaped'
113 glycerol monoalkyl glycerol tetraethers (H-GMGTs) found in thermophilic archaeal taxa
114 (Morii et al., 1998; Schouten et al., 2008a), although H-GMGT-0 may also have non-
115 thermophilic origins (Schouten et al. 2013). Whether the C_{80} tetraacids are degradation
116 products of H-GMGTs or actually bio-surfactants directly synthesized by Archaea living

117 in the crude oil remains ambiguous (Lutnaes et al., 2006, 2007). To date, isoprenoidal
118 tetracarboxylic acids have not been detected in archaeal cells.
119
120 Based on the distribution patterns of newly identified series of GDGT degradation
121 products in sedimentary samples (hydrothermally overprinted sediments from the
122 Guaymas Basin and a hot spring in China, Miocene seep carbonates, and marine
123 subsurface sediments), cell extracts and hydrolysis experiments, here we construct a
124 precursor-product reaction network from GDGTs to alcoholic and carboxylic acid
125 biphytane derivatives. Additionally, through the identification of five types of putative
126 intermediates in the sediment from Guaymas Basin, we provide strong support for the
127 hypothesis that isoprenoidal C_{80} to C_{82} tetraacids are derived from step-wise degradation
128 of 'H-shaped' GMGTs.
129

130 # 2. MATERIALS and METHODS

131

132 ## 2.1. Sample collection and preparation

133

134 *N*. *maritimus* strain SCM1 was grown aerobically at 28 °C and pH 7.5 in 8.5 l HEPES-
135 buffered Synthetic Crenarchaeota Medium (1.5 mM NH_4Cl; Könneke et al., 2005;
136 Martens-Habbena et al., 2009). The medium was inoculated with 5% of a mid-
137 logarithmic phase pre-culture of *N*. *maritimus*. Biomass was harvested early and late in
138 the growth phase as well as early and late in the stationary phase (one batch for each
139 time-point) using cross-flow filtration (Elling et al., 2014). Purity of the culture was

checked daily by phase contrast microscopy. Growth was monitored by measuring nitrite formation photometrically (Stickland and Parsons, 1972) and by counting 2% formaldehyde-fixed, SYBR Green I stained cells (Lunau et al., 2005) at the beginning and the end of the experiment. Lipids were extracted from each batch following a modified Bligh and Dyer protocol as described previously (Sturt et al., 2004; Elling et al., 2014).

The Marmorito seep carbonate samples (Marmorito limestone; see also Peckmann et al., 1999) were taken close to the village of Marmorito, in the Monferrato hills close to Torino, Italy. The Marmorito limestone is composed of dolomite and calcite, and is embedded in Miocene strata chiefly consisting of siliciclastic sediments that were deposited in a marine shelf environment. Rock samples from the vicinity Marmorito, comprising not only the so-called Marmorito limestone, are among the early examples where methane-seepage, fossil chemosynthetic benthic communities, molecular fossils, and methane-related carbonate precipitation have been described (e.g., Clari et al., 1988, 1994; Peckmann et al., 1999; Thiel et al., 1999). Apart from the characteristic molecular fossils of the consortium mediating the anaerobic oxidation of methane, biomarkers of aerobic methanotrophic bacteria were also found (Peckmann et al., 1999; Birgel and Peckmann, 2008). A detailed list of compounds identified in the Marmorito limestone and a description of the applied decalcification procedure can be found in Birgel and Peckmann (2008) and references therein. Lipid extraction was performed as described in Birgel et al. (2006).

163 The Guaymas Basin sediment sample was retrieved during the *RV Atlantis* cruise AT15-
164 56 to the Guaymas Basin, Gulf of California, Mexico, during *Alvin* dive 4568 (November
165 22 to December 6 2009, 27° 00.449' N, 111° 24.347' W). The sample came from an oil-
166 impregnated hydrothermally active area, where sedimentary temperature steeply
167 increased from ~3 °C to ~100 °C within 35 cm (Gutierrez et al., 2015). The sample was
168 surface sediment (0-4 cm depth) with the highest temperature at time of sampling
169 reaching ~12 °C. However, due to the dynamic nature of the hydrothermal activity and
170 the upward flux of fluids in the Guaymas Basin (Pearson et al., 2005), it is likely that the
171 sample has been previously heated to higher temperatures and/or contains extractable
172 organic matter formed in deeper layers at higher temperatures. Wet sediment (15-20 g)
173 was extracted using the modified Bligh and Dyer method (Sturt et al., 2004). To
174 minimize the heavy background of oil contaminants, an aliquot of the total lipid extract
175 (TLE) was cleaned with the Hybrid SPE®-Phospholipid cartridges before LC-MS
176 analysis according to the method described by Zhu et al. (2013a).
177
178 Two further sediment samples, including a marine subsurface sediment (Leg201-1227;
179 Hole 1227A, mixed from five samples: 1227A-2H2-65-75cm, 1227A-2H5-83-93cm,
180 1227A-3H2-55-65cm, 1227A-11H2-118-128m, 1227A-13H3-0-15cm; spanning from
181 8.1-113.6 m below sea floor) and a hot spring sediment (T-15, see sample description in
182 SI) were also extracted with the Bligh and Dyer method for lipid analysis.
183
184 **2.2. Lipid analysis**
185

186 For lipid analysis by normal phase liquid chromatography (NP-LC), an aliquot of TLE of
187 each sample was dissolved in *n*-hexane/isopropanol (99.5:0.5 v/v) for injection.
188 Compound separation was performed on a Dionex Ultimate 3000 RS UHPLC system
189 (Thermo Scientific, Bremen, Germany) at 50 °C, following the recently developed
190 tandem column protocol (Becker et al., 2013) using two ACQUITY UPLC® BEH Hilic
191 Amide columns (2.1 x 150 mm, 1.7 µm, Waters). Solvent gradient was programmed for a
192 constant flow rate of 0.5 mL min^{-1} and a linear increase from 3% B to 20% B in 20
193 minutes, and then linearly to 50% B at 35 minutes, after then up to 100% B at 45 min,
194 holding for 6 minutes, finally back to 3% B for 9 minutes to re-equilibrate the column,
195 where A was *n*-hexane and B was *n*-hexane/isopropanol (90:10). Detection was achieved
196 with a Bruker Maxis accurate-mass quadrupole time-of-flight (qTOF) mass spectrometer
197 (Bruker Daltonik, Bremen, Germany) coupled to the UHPLC via an atmospheric pressure
198 chemical ionization (APCI) interface run in positive ion mode. APCI source parameters
199 were as follows: corona current 3500 nA, nebulizer gas pressure 5 bar, drying gas flow 8
200 L min^{-1}, drying gas (N_2) temperature 160 °C, vaporizer temperature 400 °C. The scan
201 range was 150-2000 m/z at a rate of 2 Hz. Lipids were identified based on accurate mass
202 (better than 1 ppm), retention times and diagnostic fragments and under consideration of
203 general GDGT mass spectral features (e.g., Liu et al., 2012b), and quantified by
204 measurement of $[M+H]^+$ responses, with a extraction window of individual ion
205 chromatograms of ± 0.01 *m*/*z* units.
206
207 For the detection of carboxylic acid derivatives, reversed phase (RP) LC-MS (cf. Zhu et
208 al., 2013b) was applied with the same LC system using an ACE3 C_{18} column (2.1 × 150

209 mm, 3 µm; Advanced Chromatography Technologies Ltd., Aberdeen, Scotland) coupled
210 with a guard cartridge and maintained at 45 °C, and the same mass spectrometer (qTOF)
211 equipped with an electrospray ionization (ESI) source and operated in positive mode
212 (Bruker Daltonik, Bremen, Germany). An aliquot of TLE of each sample was dissolved
213 in methanol prior to injection. Separation of compounds was achieved isocratically with
214 100% eluent A for 10 min, followed by a rapid gradient to 24% B in 5 min, and then a
215 slow gradient to 65% B in 55 min at a flow rate of 0.2 mL min^{-1}, where the eluent A was
216 methanol/formic acid/14.8 M NH_{3aq} (100:0.04:0.10, v/v/v) and B was 2-propanol/formic
217 acid/14.8 M $NH_{3(aq)}$ (100:0.04:0.10, v/v/v). After each run, the column was washed with
218 90% B for 10 min and subsequently re-equilibrated with 100% A for another 10 min. The
219 ESI-MS conditions were set as capillary voltage 4500 V, nebulizing gas (N_2) pressure 0.8
220 bar, and dry gas (N_2) 4 L min^{-1} at a temperature of 200 °C.
221

222 # 3. RESULTS

223

224 ## 3.1. Structural elucidation of products of GDGT breakdown

225

226 Table 1 provides an overview of 19 distinct compound classes observed in this study.
227 Structural assignments are based on formulae established from accurate mass
228 measurements, chromatographic behavior and tandem mass spectrometry (MS^2) (Fig. 1, 2
229 and 3 and S1a-d contain data showing detailed MS^2 fragmentation patterns). Many
230 compounds remain only tentatively identified. Identifications of the hydroxyl derivatives,
231 including GDGTol (glycerol dialkyl glycerol triether alcohol), GMGD (glycerol

232 monobiphytanyl glycerol diether), GDD (glycerol dibiphytanol diether), GMM (glycerol
233 monobiphytanol monoether) and bpdiol (biphytanic diol), were additionally confirmed by
234 examination of products released after acidic degradation of purified GDGT-0
235 (compound compositions are given in Fig. S2, and see experiment description in SI). The
236 identification of the H-tetrol was additionally supported by the co-injection of an H-tetrol
237 mixture synthesized by reduction of the corresponding acids, which were isolated and
238 characterized by NMR spectroscopy previously (Lutnaes et al., 2007; Fig. S3, preparation
239 described in SI). C_{39} isoprenoids were assigned based on chromatographic behavior,
240 molecular formulae generated from accurate mass measurements and characteristic
241 fragment ions (MS^2 fragmentation patterns are shown in Fig. S1a). For example, the two
242 isomers of GDGTol-0 (highlighted with green circles in Fig. 3e) eluted earlier than those
243 of $C_{40/39}$-GDGTA-0 (two pink solid line circles in Fig. 3e). In addition, GDGTol-0 and
244 $C_{40/39}$-GDGTA-0 also have measurably different molecular masses, $[M+H]^+$ of m/z:
245 1320.3312 and 1320.2930, respectively and these afford calculated formulae of
246 $C_{86}H_{175}O_7^+$ for GDGTol-0 and $C_{85}H_{171}O_8^+$ for $C_{40/39}$-GDGTA-0. To add weight to this
247 assignment, the fragment ion of m/z: 651.6245 in the MS^2 of $C_{40/39}$-GDGTA-0 compared
248 to m/z: 665.6391 of GDGTA-0 represents the loss of methylene from the biphytane (Fig.
249 S1a).
250
251 **3.2. Terminally hydroxylated biphytanyl derivatives**
252
253 Hydrolysis of the glycerol ether bonds in isoprenoidal GDGT generates five types of
254 biphytane-based alcohols, with and without the glycerol backbones, namely, GDGTol,

GMGD, GDD, GMM and bpdiol (compound structures are given in Fig. S2). For example, we demonstrate their structural relationships to acyclic caldarchaeol, GDGT-0, with a parallel glycerol configuration, a distribution observed in a seep carbonate sample from Marmorito (Fig. 1a and b). Constitutional isomers, which are labeled as peak 'a' and 'b' in the chromatogram of GDGTol, GMGD and GMM in Fig. 1, represent different combinations of *sn*-2 or *sn*-3 glycerol ether bonding. Degradation products of the ring-containing GDGTs are more numerous, due to different possible arrangements of a ring on the biphytanyl chains. A detailed isomeric study of GDGTol, GMGD and GMM and their implications will be discussed in our following works. As for H-GMGTs, which have two biphytane chains linked by a bis-methylene C-C bond at position C_{20} (Lutnaes et al., 2006; 2007) the cleavage of two glycerol units results in a C_{80} H-tetrol, instead of two biphytanic diols (bpdiols). These hydroxyl derivatives of GDGT were either all, or at least some, present in our sample set comprising extracts of marine sediment, seep carbonate, hydrothermal vent, hot spring sediment and archaeal cell extract (Table 1).

3.3. Terminally-carboxylated biphytanyl derivatives

Carboxylic acids, corresponding to each of hydroxyl derivatives mentioned above, could logically be generated by oxidation of each terminal alcohol of the biphytane. These were also detected in the analyzed samples and are subsequently referred to as GDGTA for the carboxyl analogue of GDGTol and GMMA for GMM (Fig. 1a, b and Table 1). For isoprenoids possessing two primary hydroxyl groups, such as GDD and bpdiol, both mono- and dicarboxyl analogues were detected, with the monocarboxyl derivative of

GDD termed GDDA, the dicarboxyl derivative GDDAA, as well as biphytane mono- and diacids. In the case of GMGD, which does not possess a primary biphytane-bound hydroxyl group, no acid derivatives were detected. In the case of H-tetrol, which contains four primary hydroxyl groups on its two linked bpdiols, we detected mono-, di-, tri- and tetraacids in an oily sediment sample collected from a hydrothermal vent site in Guaymas Basin (Fig. 2).

Under APCI conditions, the ionization patterns of biphytanic monoacid/monool (bpmonoacid/ol) and biphytanic diacids (bpdiacid) differed from bpdiols. A protonated molecular ion $[M+H]^+$ was usually the major ion in mass spectra of bpdiols, while the acids produced more complex mass spectra in our analyses. Dehydrated molecular ions and unknown adducts were formed during the ionization of carboxyl derivatives (Fig. 1b and S1d). The main adduct ions detected were $[M+H+42]^+$ for bpmonoacid/ol and $[M+H+84]^+$ for bpdiacids (Fig. S1d).

3.4. C_{39} and C_{38} isoprenoids

In addition to the series of hydroxylated and carboxylated C_{40} biphytane derivatives, we identified some with shortened alkyl chains such as the C_{39} analogues. For example, in most analyzed samples analogues with one methylene unit less than GDGTol and GDGTA, here termed $C_{40/39}$-GDGTol and $C_{40/39}$-GDGTA (Arabic numbers represent the carbon number of the two isoprenoidal chains in the molecule), always co-occurred at lower abundance with their $C_{40/40}$ analogues (Fig. 3b, e). C_{39} derivatives were also

301 detected as analogues of GDD, bpdiol and GMM (Fig. 3a, c and d). Additionally, we
302 detected signals that we attribute to the pseudo-homologue of C_{38} isoprenoids, as
303 GDGTol and GDD (Fig. 3a and b). Within the group of GDDs reduced by two C-atoms,
304 we observed both $C_{39/39}$ and $C_{40/38}$ derivatives (Fig. 3a). Three isomers of the acyclic and
305 four isomers of crenarchaeol-related GDD were detected (Fig. 3a). In previous studies
306 ^{13}C depleted C_{39} head-to-head linked isoprenoids were detected in Cretaceous (Sandy et
307 al., 2012) and Carboniferous seep carbonates (Birgel et al., 2008b); those compounds
308 presumably represent the hydrocarbon derivatives of the C_{39} functionalized compounds
309 found in this study. Interestingly, no derivatives of C_{80} H-tetrol and tetraacid with
310 reduced carbon chains were detected in our samples.
311

312 # 4. DISCUSSION

313

314 ## 4.1. The occurrence of GDGT degradation derivatives in environmental samples

315

316 The distributions of major degradation derivatives of GDGT-0 and H-GMGT-0 were
317 compared in four representative environmental samples (Fig. 4), which include modern to
318 late Miocene marine subsurface sediment (Leg201-1227), modern hot spring (T-15) and
319 hydrothermally heated sediment (Guaymas Basin 4568), and the Miocene Marmorito
320 seep carbonate. Distinct patterns of degradation derivatives in these four types of samples
321 from different environments and of different age (modern sediments and ancient
322 carbonate rock) reflect variable degrees of degradation and preservation.
323

4.1.1. Distributions of regular GDGT degradation products in environmental samples

The distributions of GDGT degradation products across our sample set suggest that the biological sources of GDGTs, as well as the debris depositional histories, influence the diagenetic trajectory of GDGTs. By way of example, the degradation derivatives of GDGT-0 are around twice as abundant as their precursor in the marine sediment sample of Leg 201-1227, in which bpdiol-0 comprises over half of all of the detected degradation products (Fig. 4). However, the GDGT degradation derivatives in Miocene seep carbonates exhibited a lower overall relative abundance, but with a greater variety and portion of relatively labile components, such as the carboxyl derivatives (Table 1 and Fig. 4). Regular isoprenoidal GDGTs (as compared to H-GMGTs) preserved in marine sediments are primarily derived from planktonic archaea, dwelling in the water column. In contrast, those in seep carbonates receive a larger *in-situ* contribution from benthic communities engaged in anaerobic oxidation of methane (AOM), as confirmed by low $\delta^{13}C$ values of biphytanic diacids (cf. Birgel et al., 2008a). The higher proportion of degradation derivatives relative to their GDGT precursors in deep subsurface sediment apparently results from long-term degradation under mild to moderate degradation conditions, with prolonged degradation compared to the Marmorito seep site. Such a long-term diagenetic process is consistent with the influence of the coexisting deep biosphere, which can prevail over many millions of years (e.g. Inagaki et al., 2015). The extraordinarily good preservation of labile compounds in seep carbonates can be attributed to significant *in-situ* GDGT production combined with co-eval carbonate formation and resulting early lithification within methane seepage systems (e.g.,

Peckmann et al., 1999; Birgel et al., 2008a), rather than representing input from various sedimentary or sedimentary/planktonic archaea (cf. Feng et al., 2014; Birgel et al., 2008a).

The relative abundance of degradation products in Guaymas basin sediment is over 40% of all GDGT-derived compounds (Fig. 4). Both biodegradation and thermal diagenesis can be potential sources of degradation products, due to the presence of both active microbial communities and high temperature hydrothermal fluids in Guaymas basin sediments (Teske et al., 2014; Gutierrez et al., 2015). In contrast, there are only low abundances of GDD and bpdiol (< 10%) detected as GDGT degradation products in the hot spring sediment (Fig. 4).

In addition to the contrasting patterns of the different environments, there is a compositional discrepancy between each class of GDGT product within the same sample. For example, previous studies that documented the presence of bpdiols and bpdiacids in environmental samples have shown that the ring distributions and carbon isotopic compositions differ for biphytanes released from coexisting GDGTs (Schouten et al., 1998; Birgel et al., 2008a; Saito and Suzuki, 2010). The Marmorito limestone samples (Fig. 5; Birgel et al. (2008a) provide results on hydrocarbons and bpdiacids), show distinct ring distribution patterns for GDGT, bpdiol, bpmonoacid/ol and bpdiacid; GDGTs are dominated by GDGT-0 and crenarchaeol, while the relative abundance of tricyclic biphytane derivatives derived from crenarchaeol gradually decreases for the hydroxyl to carboxyl products. Multiple inputs, combined with selective preservation could cause such distributional differences. The ring distribution of GDGTs preserved in

sediments may reflect a mixed contribution from both planktonic and benthic species and is frequently dominated by compounds from planktonic sources (Wuchter et al., 2005; Huguet et al., 2007; Lengger et al., 2012). Planktonic and sedimentary archaeal communities could contribute different lipids. Further, compared to biphytanyl products derived from benthic species within the sediment, those derived from the water column will have experienced a very different transportation history. This might explain why the tricyclic diacid derived from planktonic archaea are rare, while the acyclic, mono- and bicyclic diacids with origins from sedimentary methanotrophic archaea, are more common and more ^{13}C-depleted in the seep carbonate (isotopic data published in Birgel et al., 2008a).

4.1.2. The degradation of H-GMGTs to H-tetrols and H-tetraacids

H-GMGT-0 and its hydroxylated degradation products are generally present in the samples from low-temperature and hydrothermal environments (Table 1 and Fig. 4), while compounds with multiple cycloalkyl groups and additional methylations are restricted to the hydrothermal samples alone. In low-temperature samples, H-GMGT-0 is far more abundant than H-GMD-0 (acyclic H-shaped glycerol monoalkyl diether) and tetrol-0 (Fig. 4). The apparently different patterns of H-GMGT-0 and its derivatives, compared to GDGT-0 and its highly abundant degradation products, point to contributions of distinct species and/or different diagenetic pathways.

392 We detected H-tetrol and H-tetraacids, and their partially oxidized 'H-shaped' mono-, di-
393 and triacid intermediates, in the oily Guaymas Basin sediment (Fig. 2). The occurrence of
394 partially oxidized intermediates, such as the mono-, di- and triacids is more likely a
395 selective and stepwise reaction with enzymatic catalysis rather than chemical diagenesis.
396 H-tetraacids accumulated in naphthenate deposits in oil well infrastructure and pipelines
397 and in crude oils, have distributions usually dominated by 4-8 cyclopentyl rings and 1 or
398 2 additional methyl substitutions (Lutnaes et al., 2007; Sutton & Rowland, 2014).
399 Although H-GMGT-0 is known to be present in a broad range of mesophilic
400 environments (Schouten at al., 2008a), those with multiple cyclizations and methylations
401 have been only detected in hyperthermophilic archaeal species (Schouten et al., 2008b;
402 Knappy et al., 2011; Liu et al., 2012b). H-GMGTs with multiple cyclizations and
403 methylations were detected in both hot spring and Guaymas Basin sediments analyzed.
404 However, H-tetraacids were only found in the oil-impregnated Guaymas Basin sediment
405 (Table 1). In addition to the diagenetic contribution, Lutnaes et al. (2006) also speculated
406 that these tetraacids might be produced by thermophilic, oil-degrading archaea as
407 biosurfactants to facilitate their metabolism. Additional studies would be required to test
408 this hypothesis rigorously. Given the occurrence of biphytane, C_{39} and smaller head-to-
409 head linked isoprenoids in the geological record, C_{80} based H-shaped isoprenoidal
410 hydrocarbons might also exist. Whilst these are not detectable with conventional GC-MS,
411 they would be amenable to high temperature GC-MS (cf. Sutton & Rowland, 2012)
412
413 **4.2. The occurrence of GDGT degradation derivatives in archaeal cell extracts**
414

In a previous study concerning the characterization of GDD, Liu et al. (2012a) observed the existence of core GDD in the cell extracts of the methanogen *Methanothermococcus thermolithotrophicus*. More recently, Meador et al. (2014) reported detection of both core and monoglycosidic GDD (1G-GDD) in a culture of the planktonic ammonia oxidizer *N. maritimus*. Here we extend these observations and report newly identified biphytane derivatives in fresh biomass collected at different growth phases of cell extracts of the archaeon *N. maritimus*. Core lipids accounted for 8.2-15% of the total detected lipids during different growth phases (Elling et al., 2014). We selected the most abundant component, crenarchaeol, to illustrate the distribution of its hydroxyl and carboxyl derivatives in different growth phases. GDD-Cren. and bpdiol-Cren. were the only detected hydroxyl components during early exponential growth (Fig. 6); they jointly accounted for less than 1% of all crenarchaeol-based derivatives. In the late growth phase, however, the relative abundances of GDD-Cren. and bpdiol-Cren. were almost doubled, while the acid (GDDA-Cren.) and a C_{39} component ($C_{40/39}$-GDD-Cren.) emerged as well. GDD-Cren., depleted by two methylene units ($C_{39/39}$ and $C_{40/38}$-GDD-Cren.), together with GDGTol-Cren. were only observed in the stationary phase.

Although these derivatives occurred in cell extracts, they cannot be simply attributed as intermediates of GDGT biosynthesis. For example, the carboxyl and C_{39} based derivatives, such as GDDA and $C_{40/39}$-GDD, are more likely further oxidized products of GDD. For example, archaeal biphytanyl moieties, synthesized via the mevalonic acid (MVA) or methylerythritol phosphate (MEP) pathways, should have a carbon number that is a multiple of five. Accordingly, the most plausible formation pathway for the C_{38}

438 and C_{39} moieties is oxidation and decarboxylation of C_{40} precursors. Formation of C_{38}
439 and C_{39} moieties via degradation of C_{40} biphytanyl moieties is also consistent with the
440 higher relative abundance of GDDA and $C_{40/39}$-GDD during the late stationary phase (Fig.
441 6). The loss of one methylene unit represents an α-oxidation step. A similar well-known
442 enzymatic α-oxidation of isoprenoids is that of phytanic acid (C_{20}) to pristanic acid (C_{19})
443 by a wide range of organisms (e.g., Rontani and Volkman, 2003; Jansen and Wanders,
444 2006, and other studies cited therein). As in phytanic acid, the C_3 methyl group in
445 biphytanic acid (C_{40}) derivatives prevents an initial β-oxidation mechanism; instead,
446 these compounds undergo α-oxidation to yield C_{39} based carboxyl isoprenoids. In such a
447 scenario the production of GDD and GDGTol consisting of C_{38} derivatives would require
448 two successive α-oxidation steps. This is inconsistent with the reported α-oxidation of
449 phytanic acid, which is followed by hydroxylation and then β-oxidation (e.g. Jansen and
450 Wanders, 2006, and other studies cited therein). Therefore, elucidation of the degradation
451 process leading to a C_{38} isoprenoid requires further study. Furthermore, α- as well as β-
452 oxidation would only result in carboxyl derivatives, and could not explain the occurrence
453 of hydroxyl analogues, such as $C_{40/39}$-GDD and $C_{40/39}$-GDGTol (Fig. 3). Although the
454 detection of carboxyl derivatives and C_{38} and C_{39} based isoprenoids in a metabolic active
455 culture of *N. maritimus* may imply an intracellular modification of existing C_{40} based
456 lipids, probably as a result of cell senescence, their contribution is less than 2% of the
457 core lipid fraction, or approximately 0.01% of the entire lipidome. The exact mechanisms
458 responsible for the remarkable proportions (up to 70% in the marine subsurface sediment,
459 Leg201-1227, Fig. 4) of degradation products in environmental samples remain
460 unresolved. The presence of degradation products in archaeal cell extracts, as well as

their increase towards later growth and stationary phases, suggests that some are formed rapidly and probably via enzymatic catalysis. On the other hand, the high proportion and diversity of degradation products in the hydrothermally influenced settings also leaves room for an additional role of abiotically-mediated chemical degradation reactions, at least for some of the speculated steps leading via catagenesis from GDGTs to biphytanyl hydrocarbons (cf. Rowland, 1990).

4.3. Evidence of analogous behavior of non-isoprenoidal GDGTs

Non-isoprenoidal GDGTs, such as the hypothetical hybrid isoprenoidal/branched GDGT (IB-GDGT) and branched GDGTs, are known to be widely distributed in various environments, although their exact structures and biological source(s) remain unknown (Liu et al., 2012b). The degradation pathways described here are not limited to archaeal GDGTs. For example, in one of the seep carbonate samples, which contains high abundances of branched and IB-GDGTs, non-isoprenoidal GDDs, GMMs and diols have been detected. These possibly represent degradation products of the corresponding branched and IB-GDGTs in the same deposit (Fig. S4 and S5). Our analytical methods also reveal the presence of carboxyl derivatives of these lipids. Non-isoprenoidal GDGTol, GDGTA, GMGD, and their corresponding products with reduced carbon chains (loss of one or two methylene units) were not identified, however, and we attribute this to their low overall abundance in the analyzed samples.

5. CONCLUSIONS

As with other lipid classes, the intact archaeal tetraethers released from the cells of defunct archaea into various depositional settings, are subjected to diagenesis in sediments. We detected three major classes of GDGT degradation products comprising biphytanyl molecules with terminal hydroxyl, terminal carboxyl and shortened carbon chains. A hypothetical scheme of the GDGT degradation pathway to rationalize such a pathway is illustrated in Fig. 7. The labile polar head groups of intact GDGTs, as they occur in living cells, are initially lost to produce the more recalcitrant core GDGTs. Hydrolysis of the different ether bonds then, as we suggest, results in discrete series of hydroxyl derivatives composed of one or two glycerol and biphytanol units. Oxidation of each terminal hydroxyl functional group may then generate related carboxyl products. Elimination of the C_1 carbon via α-oxidation and subsequent β-oxidation steps, will likely convert the C_{40} biphytanyl based compounds into shortened isoprenoids, such as $C_{40/39}$-GDGTA and $C_{40/39}$-GDGTol. Further chemical or biological alteration of these intermediates may over geological time, result in the C_{40}, C_{39} and smaller head-to-head linked isoprenoidal hydrocarbons reported to occur in petroleum and marine deposits.

A multitude of diagenetic processes will lead to the degradation of GDGTs in sediments. However, we also observed the accumulation of C_{39} based carboxyl isoprenoids in the later growth and stationary phases of an archaeal cell culture. This implies that enzymatic pathways for degradation of GDGTs also exist, very likely, as a response to substrate limitation, senescence or cell lysis. Additional studies will be required to study this facet in greater detail.

507 The detection of H-GMGT, H-GMD, H-tetrols and their further oxidized carboxyl
508 intermediates in the oil-contaminated sediments of Guaymas Basin elucidated a
509 formation pathway from H-GMGT to H-tetraacids under anoxic conditions.
510 Metagenomic data for samples from the Guaymas Basin and especially sediment with oil
511 impregnation may help to elucidate the origin of H-tetraacids further.
512
513 In various geological settings these hydroxyl and carboxyl derivatives co-occur with their
514 GDGT precursors, including both isoprenoidal and non-isoprenoidal GDGTs. Our
515 analysis of their distributions in environmental samples and archaeal cell extracts
516 represents an initial effort to document the possible diagenetic pathways of GDGTs and
517 to bring about the same level of understanding that we have for steroids and triterpenoids.
518

519

ACKNOWLEDGEMENTS

521

522 X.-L.L. was funded by European Union's Seventh Framework Programme–"Ideas"
523 Specific Programme, ERC grant agreement No. 247153 (Advanced Grant DARCLIFE;
524 PI K.-U.H.), the Simons Foundation Collaboration on the Origins of Life (SCOL).
525 Cultivation experiments and lipid analyses at the University of Bremen were funded by
526 the Deutsche Forschungsgemeinschaft through the Gottfried Wilhelm Leibniz Prize
527 awarded to K.-U.H. (Hi 616-14-1). SJR and PAS were funded by a European Research
528 Council Advanced Investigators Award to SJR for project OUTREACH (agreement no.
529 228149). We thank Dr. Ann Pearson, Dr. Yoshinori Takano and two anonymous
530 reviewers for their constructive comments on this work.

531

REFERENCES

Baugh T.D., Wolf N.O., Mediaas H., Vindstad J.E. and Grande K. (2004) Characterization of a Calcium Naphthanate Deposit -The ARN Acid Discovery. Preprints/American Chemical Society, Division of Petroleum Chemistry **49**, 274−276.

Baugh T.D., Grande K.V., Mediaas H., Vindstad J.E. and Wolf N.O. (2005) In The Discovery of High Molecular Weight Naphthenic Acids (ARN Acid) Responsible for Calcium Naphthenate Deposits. SPE International Symposium on Oilfield Scale, Aberdeen, U.K., May 11−12 2005; SPE 93011.

Becker K.W., Lipp J.S., Zhu C., Liu X.-L. and Hinrichs K.-U. (2013) An improved method for the analysis of archaeal and bacterial ether core lipids. *Org*. *Geochem*. **61**, 34-44.

Birgel, D., Thiel, V., Hinrichs, K.-U., Elvert, M., Campbell, K.A., Reitner, J., Farmer, J.D. and Peckmann, J. (2006) Lipid biomarker patterns of methane-seep microbialites from the Mesozoic convergent margin of California. *Org*. *Geochem*. **37**, 1289–1302.

Birgel, D. and Peckmann, J. (2008) Aerobic methanotrophy at ancient marine methane seeps: a synthesis. *Org*. *Geochem*. **39**, 1659–1667.

Birgel D., Elvert M., Han X. and Peckmann J. (2008a) ^{13}C-depleted biphytanic diacids as tracers of past anaerobic oxidation of methane. *Org*. *Geochem*. **39**, 152–156.

Birgel, D., Himmler, T., Freiwald, A. and Peckmann, J. (2008b) A new constraint on the antiquity of anaerobic oxidation of methane: Late Pennsylvanian seep limestones from southern Namibia. *Geology* **36**, 543–546.

Brocks J.J. and Schaeffer P. (2008) Okenane, a biomarker for purple sulfur bacteria (Chromatiaceae), and other new carotenoid derivatives from the 1640 Ma Barney Creek Formation. *Geochim*. *Cosmochim*. *Acta* **72**, 1396–1414.

Chappe B., Albrecht P. and Michaelis W. (1982) Polar lipids of archaebacteria in sediments and petroleums. *Science* **217**, 65–66.

Clari P., Gagliardi C., Governa M.E., Ricci B. and Zuppi G.M. (1988) I calcari de Marmorito: Una testimonianza di processidiagene- tici in presenza di metano. *Boll Museo Regionale Sci Naurali Torino* **6**, 197–216.

Clari P., Fornara L., Ricci B. and Zuppi G.M. (1994) Methane-derived carbonates and chemosymbiotic communities of Piedmont (Miocene, northern Italy): an update. *Geo-Marine Lett*. **14**, 201–209.

Elling F.J., Könneke M., Lipp J.S., Becker K.W., Gagen E.J. and Hinrichs K.-U. (2014) Effects of growth phase on the membrane lipid composition of the thaumarchaeon *Nitrosopumilus maritimus* and their implications for archaeal lipid distributions in the marine environment. *Geochim*. *Cosmochim*. *Acta* **141**, 579–597.

569 Feng D., Birgel D., Peckmann J., Roberts H. H., Joye S. B., Sassen R., Liu X.-L.,
570 Hinrichs K.-U. and Chen D. (2014) Time integrated variation of sources of fluids and
571 seepage dynamics archived in authigenic carbonates from Gulf of Mexico Gas
572 Hydrate Seafloor Observatory. *Chem*. *Geol*. **385**, 129–139.

573 Gutierrez, T., Biddle, J.F., Teske, A. and Aitken, M.D. (2015) Cultivation-dependent and
574 cultivation-independent characterization of hydrocarbon-degrading bacteria in
575 Guaymas Basin sediments. *Front*. *Microbiol*. **6**, doi: 10.3389/fmicb.2015.00695

576 Harvey, H.R., Fallon, R.D. and Patton, J.S. (1986) The effect of organic matter and
577 oxygen on the degradation of bacterial membrane lipids in marine sediments.
578 *Geochim*. *Cosmochim*. *Acta* **50**, 795–804.

579 Huguet, C., Schimmelmann, A., Thunell, R., Lourens, L.J., Sinninghe Damsté, J.S. and
580 Schouten, S. (2007) A study of the TEX_{86} paleothermometer in the water column and
581 sediments of the Santa Barbara Basin, California. *Paleoceanography* **22**,
582 doi:10.1029/2006PA001310

583 Inagaki, F., et al. (2015), Exploring deep microbial life in coal-bearing sediment down to
584 2.5 km below the ocean floor, *Science*, **349**, 420–424,

585 Innes, H.E., Bishop, A.N., Head, I.M. and Farrimond, P. (1997) Preservation and
586 diagenesis of hopanoids in Recent lacustrine sediments of Priest Pot, England. *Org*.
587 *Geochem*. **26**, 565-576.

588 Jansen G.A. and Wanders R.J.A. (2006) Alpha-Oxidation. *Biochim Biophys Acta – Mol*.
589 *Cell* **1763**, 1403–1412.

590 Könneke M., Bernhard A. E., de la Torre J. R., Walker C. B., Waterbury J. B. and Stahl
591 D. A. (2005) Isolation of an autotrophic ammonia-oxidizing marine archaeon.
592 *Nature* **437**, 543–546.

593 Knappy, C.S., Nunn, C.E.M., Morgan, H.W. and Keely, B.J. (2011) The major lipid cores
594 of the archaeon *Ignisphaera aggregans*: implications for the phylogeny and
595 biosynthesis of glycerol monoalkyl glycerol tetraether isoprenoid lipids.
596 *Extremophiles* **15**, 517–528.

597 Knappy C.S. and Keely B.J. (2012) Novel glycerol dialkanol triols in sediments:
598 transformation products of glycerol dibiphytanyl glycerol tetraether lipids or
599 biosynthetic intermediates? *Chem. Commun.* **48**, 841–843.

600 Kuypers, M. M. M., Blokker, P., Erbacher, J., Kinkel, H., Pancost, R. D., Schouten, S. and
601 Sinninghe Damsté, J. S. (2001) Massive expansion of marine Archaea during a
602 mid-Cretaceous oceanic anoxic event. *Science* **293**, 92-95.

603 Lengger, S.K., Hopmans, E.C., Reichart, G.-J., Nierop, K.G.J., Damsté, J.S.S. and
604 Schouten, S. (2012) Intact polar and core glycerol dibiphytanyl glycerol tetraether
605 lipids in the Arabian Sea oxygen minimum zone. Part II: Selective preservation and
606 degradation in sediments and consequences for the TEX_{86}. *Geochim*. *Cosmochim*.

607 *Acta* **98**, 244–258.

608 Lipp J.S. and Hinrichs K.-U. (2009) Structural diversity and fate of intact polar lipids in
609 marine sediments. *Geochim*. *Cosmochim*. *Acta* **73**, 6816–6833.

610 Liu, X.-L., Lipp, J.S. and Hinrichs, K.-U. (2011) Distribution of intact and core GDGTs
611 in marine sediments. *Org*. *Geochem*. **42**, 368–375.

612 Liu X.-L., Lipp J.S., Schröder J.M., Summons R.E. and Hinrichs K.-U. (2012a)
613 Isoprenoid glycerol dialkanol diethers: A series of novel archaeal lipids in marine
614 sediments. *Org*. *Geochem*. **43**, 50–55.

615 Liu X.-L., Summons R.E. and Hinrichs K.-U. (2012b) Extending the known range of
616 glycerol ether lipids in the environment: structural assignments based on tandem
617 mass spectral fragmentation patterns. *Rapid Commun*. *Mass Spectrom*. **26**, 2295–
618 2302.

619 Lunau M., Lemke A., Walther K., Martens-Habbena W. and Simon M. (2005) An
620 improved method for counting bacteria from sediments and turbid environments by
621 epifluorescence microscopy. *Environ*. *Microbiol*. **7**, 961–968.

622 Lutnaes B.F., Brandal Ø., Sjöblom J. and Krane J. (2006) Archaeal C_{80} isoprenoid
623 tetraacids responsible for naphthenate deposition in crude oil processing. *Org*.
624 *Biomol*. *Chem*. **4**, 616.

625 Lutnaes B.F., Krane J., Smith B.E. and Rowland S.J. (2007) Structure elucidation of C_{80},
626 C_{81} and C_{82} isoprenoid tetraacids responsible for naphthenate deposition in crude oil
627 production. *Org*. *Biomol*. *Chem*. **5**, 1873.

628 Mackenzie, A.S., Brassell, S.C., Eglinton, G. and Maxwell, J.R. (1982) Chemical fossils
629 – the geological fate of steroids. *Science* **217**, 491–504.

630 Martens-Habbena W., Berube P.M., Urakawa H., de la Torre J.R. and Stahl D.A. (2009)
631 Ammonia oxidation kinetics determine niche separation of nitrifying Archaea and
632 Bacteria. *Nature* **461**, 976–979.

633 Meador T.B., Zhu C., Elling F.J., Könneke M. and Hinrichs K.-U. (2014) Identification
634 of isoprenoid glycosidic glycerol dibiphytanol diethers and indications for their
635 biosynthetic origin. *Org*. *Geochem*. **69**, 70–75.

636 Meador, T.B., Bowles, M., Lazar, C., Zhu, C., Teske, A. and Hinrichs, K.-U. (2015) The
637 archaeal lipidome in estuarine sediment dominated by members of the miscellaneous
638 Crenarchaeotal Group. *Environ*. *Microbiol*. **17**, 2441-2458.

639 Meunier-Christman C. (1988) Géochimie organique de phosphates et schistes bitumineux
640 marocains: étude du processus de phosphatogenèse. PhD thesis, University of
641 Strasbourg, p. 133.

642 Moldowan J.M. and Seifert W.K. (1979) Head-to-head linked isoprenoid hydrocarbons in

643 petroleum. *Science* **204**, 169–171.

644 Morii, H., Eguchi, T., Nishihara, M., Kakinuma, K., König, H. and Koga, Y. (1998) A
645 novel ether core lipid with H-shaped C_{80}-isoprenoid hydrocarbon chain from the
646 hyperthermophilic methanogen *Methanothermus fervidus*. *Biochim*. *Biophys*. *Acta*
647 **1390**, 339–345.

648 Peckmann, J., Thiel, V., Michaelis, W., Clari, P., Gaillard, C., Martire, L. and Reitner, J.
649 (1999) Cold seep deposits of Beauvoisin (Oxfordian; southeastern France) and
650 Marmorito (Miocene; northern Italy): microbially induced authigenic carbonates. *Int*.
651 *J*. *Earth Sci*. **88**, 60–75.

652 Pearson, A., Seewald, J.S. and Eglinton, T.I. (2005) Bacterial incorporation of relict
653 carbon in the hydrothermal environment of Guaymas Basin. *Geochim*. *Cosmochim*.
654 *Acta* **69**, 5477–5486.

655 Pearson, A. and Ingalls, A.E. (2013) Assessing the use of Archaeal lipids as marine
656 environmental proxies. *Annu*. *Rev*. *Earth Planet*. *Sci*. **41**, 359–384.

657 Pease, T.K., Van Vleet, E.S., Barre, J.S. and Dickins, H.D. (1998) Degradation of
658 glyceryl ethers by hydrous and flash pyrolysis. *Org*. *Geochem*. **29**, 979–988.

659 Peters, K. E., Walters, C. C. and Moldowan, J. M. (2004) The biomarker guide, 2nd edn.
660 Cambridge, UK: Cambridge University Press.

661 Rontani J.-F. and Volkman J.K. (2003) Phytol degradation products as biogeochemical
662 tracers in aquatic environments. *Org*. *Geochem*. **34**, 1–35.

663 Rowland, S.J. (1990) Production of acyclic isoprenoid hydrocarbons by laboratory
664 maturation of methanogenic bacteria. *Org*. *Geochem*. **15**, 9–16.

665 Sandy, M. R., Lazăr, I., Peckmann, J., Birgel, D., Stoica, M. and Roban, R. D. (2012)
666 Methane-seep brachiopod fauna within turbidites of the Sinaia Formation, Eastern
667 Carpathian Mountains, Romania. *Palaeogeogr*. *Palaeoclimatol*. *Palaeoecol*. **323-325**,
668 42-59.

669 Saito H. and Suzuki N. (2010) Distribution of acyclic and cyclic biphytanediols in recent
670 marine sediments from IODP Site C0001, Nankai Trough. *Org*. *Geochem*. **41**, 1001–
671 1004.

672 Schouten S., Hoefs M.J., Koopmans M.P., Bosch H.-J. and Sinninghe Damsté J.S. (1998)
673 Structural characterization, occurrence and fate of archaeal ether-bound acyclic and
674 cyclic biphytanes and corresponding diols in sediments. *Org*. *Geochem*. **29**, 1305–
675 1319.

676 Schouten, S., Wakeham, S. G., Hopmans, E. C. and Sinninghe Damsté, J. S. (2003)
677 Biogeochemical evidence that thermophilic archaea mediate the anaerobic oxidation
678 of methane. *Appl*. *Environ*. *Microbiol*. **69**, 1680-1686.

679 Schouten, S., Baas, M., Hopmans, E.C. and Sinninghe Damsté, J.S. (2008a) An unusual

680 isoprenoid tetraether lipid in marine and lacustrine sediments. *Org*. *Geochem*. **39**,
681 1033–1038.

682 Schouten, S., Baas, M., Hopmans, E.C., Reysenbach, A.-L. and Sinninghe Damsté, J.S.
683 (2008b) Tetraether membrane lipids of Candidatus ‘‘*Aciduliprofundum boonei*’’, a
684 cultivated obligate thermoacidophilic euryarchaeote from deep-sea hydrothermal
685 vents. *Extremophiles* **12**, 119–124.

686 Schouten, S., Hopmans, E.C. and Sinninghe Damsté, J.S. (2013) The organic
687 geochemistry of glycerol dialkyl glycerol tetraether lipids: A review. *Org*. *Geochem*.
688 **54**, 19–61.

689 Stickland J.D.H. and Parsons T.R.A. (1972) A Practical Handbook of Seawater Analysis.,
690 Fisheries Research Board of Canada, Ottawa.

691 Sturt H. F., Summons R. E., Smith K., Elvert M. and Hinrichs K.-U. (2004) Intact polar
692 membrane lipids in prokaryotes and sediments deciphered by high-performance
693 liquid chromatography/electrospray ionization multistage mass spectrometry - new
694 biomarkers for biogeochemistry and microbial ecology. *Rapid Commun*. *Mass*
695 *Spectrom*. **18**, 617–628.

696 Sutton, P.A. and Rowland, S.J. (2012) High temperature gas chromatography–time-of-
697 flight-mass spectrometry (HTGC–ToF-MS) for high-boiling compounds. *J*.
698 *Chromatogr*. *A*. **1243**, 69–80.

699 Sutton, P.A. and Rowland, S.J. (2014) Determination of the content of C_{80} tetraacids in
700 petroleum. *Energy Fuels* **28**, 5657–5669.

701 Teske, A., Callaghan, A.V. and LaRowe, D.E. (2014) Biosphere frontiers of subsurface
702 life in the sedimented hydrothermal system of Guaymas Basin. *Front*. *Microbiol*. **5**,
703 doi:10.3389/fmicb.2014.00362

704 Thiel, V., Peckmann, J., Seifert, R., Wehrung, P., Reitner, J. and Michaelis, W. (1999)
705 Highly isotopically depleted isoprenoids: molecular markers for ancient methane
706 venting. *Geochim*. *Cosmochim*. *Acta* **63**, 3959–3966.

707 Weijers, J.W.H., Schouten, S., Hopmans, E.C., Geenevasen, J.A.J., David, O.R.P.,
708 Coleman, J.M., Pancost, R.D. and Sinninghe Damsté, J.S. (2006) Membrane lipids
709 of mesophilic anaerobic bacteria thriving in peats have typical archaeal traits.
710 *Environ*. *Microbiol*. **8**, 648–657.

711 Wuchter, C., Schouten, S., Wakeham, S.G. and Sinninghe Damsté, J.S. (2005) Temporal
712 and spatial variation in tetraether membrane lipids of marine Crenarchaeota in
713 particulate organic matter: Implications for TEX_{86} paleothermometry.
714 *Paleoceanography* **20**, doi:10.1029/2004PA001110

715 Xie, S., Lipp, J.S., Wegener, G., Ferdelman, T.G. and Hinrichs, K.-U. (2013) Turnover of

716 microbial lipids in the deep biosphere and growth of benthic archaeal populations.
717 *Proc. Natl. Acad. Sci. USA* **110**, 6010-6014.

718 Yang H., Pancost R.D., Tang C., Ding W., Dang X. and Xie S. (2014) Distributions of
719 isoprenoid and branched glycerol dialkanol diethers in Chinese surface soils and a
720 loess–paleosol sequence: Implications for the degradation of tetraether lipids. *Org*.
721 *Geochem*. **66**, 70–79.

722 Yoshinaga, M.Y., Lazar, C.S., Elvert, M., Lin, Y-S., Zhu, C., Heuer, V.B., Teske, A. and
723 Hinrichs, K.-U. (2015) Possible roles of uncultured archaea in carbon cycling in
724 methane-seep sediments. *Geochim*. *Cosmochim*. *Acta*, **164**, 35-52.

725 Zhu, R., Evans, T.W., Wörmer, L., Lin, Y.-S., Zhu, C. and Hinrichs, K.-U. (2013a)
726 Improved sensitivity of sedimentary phospholipid analysis resulting from a novel
727 extract cleanup strategy. *Org*. *Geochem*. **65**, 46–52.

728 Zhu C., Lipp J.S., Wörmer L., Becker K.W., Schröder J. and Hinrichs K.-U. (2013b)
729 Comprehensive glycerol ether lipid fingerprints through a novel reversed phase liquid
730 chromatography–mass spectrometry protocol. *Org*. *Geochem*. **65**, 53–62.

Compounds	Abbreviation	Structural illustration	Distribution				
			Leg 201-1227	Marmorito seep carbonate	Guaymas Basin 4568	Hot Spring T-15	*N. maritimus* late stat. phase
glycerol dialkyl glycerol tetraether	GDGT	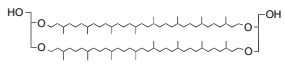	+	+	+	+	+
glycerol dialkyl glycerol triether alcohol	GDGTol	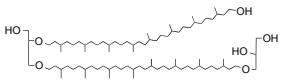	+	+	+	n.d.	+
glycerol dialkyl glycerol triether acid	GDGTA	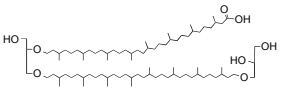	+	+	n.d.	n.d.	n.d.
glycerol dibiphytanol diether	GDD	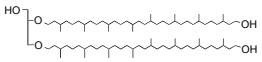	+	+	+	+	+
glycerol dibiphytanol diether monoacid	GDDA	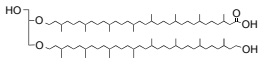	+	+	+	n.d.	+
glycerol dibiphytanol diether diacid	GDDAA	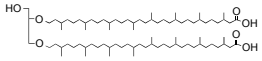	n.d.	+	n.d.	n.d.	n.d.
glycerol monobiphytanyl glycerol diether	GMGD	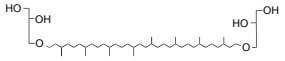	+	+	+	n.d.	n.d.
glycerol monobiphytanol monoether	GMM	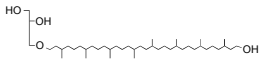	+	+	+	n.d.	n.d.
glycerol monobiphytanol monoether acid	GMMA	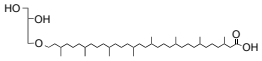	n.d.	+	n.d.	n.d.	n.d.
biphytanic diol	bpdiol	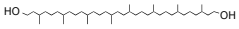	+	+	+	+	+
biphytanic monoacid	bpmonoacid/ol	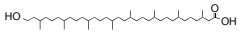	+	+	n.d.	n.d.	n.d.
biphytanic diacid	bpdiacid	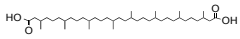	n.d.	+	n.d.	n.d.	n.d.
H-shaped glycerol monoalkyl glycerol tetraether	H-GMGT	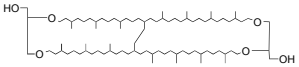	+	+	+	+	n.d.
H-shaped glycerol monoalkyl diether	H-GMD	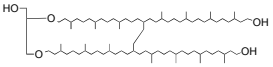	+	+	+	+	n.d.
H-shaped C_{80} tetrol	H-tetrol	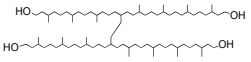	+	+	+	+	n.d.
H-shaped C_{80} monoacid	H-monoacid	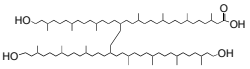	n.d.	n.d.	+	n.d.	n.d.
H-shaped C_{80} diacid	H-diacid	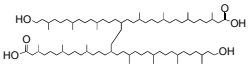	n.d.	n.d.	+	n.d.	n.d.
H-shaped C_{80} triacid	H-triacid	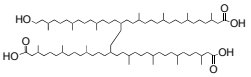	n.d.	n.d.	+	n.d.	n.d.
H-shaped C_{80} tetraacid	H-tetraacid	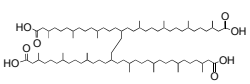	n.d.	n.d.	+	n.d.	n.d.

731

732 **Table 1.** Compound classes discussed in the paper. Illustrated structures show only the
733 acyclic biphytane derivatives. Constitutional isomers are not included. Representative
734 samples showing the distribution of GDGT and degradation products in various
735 environment settings and cell. '+' compound detected, 'n.d.' compound not detected.

736

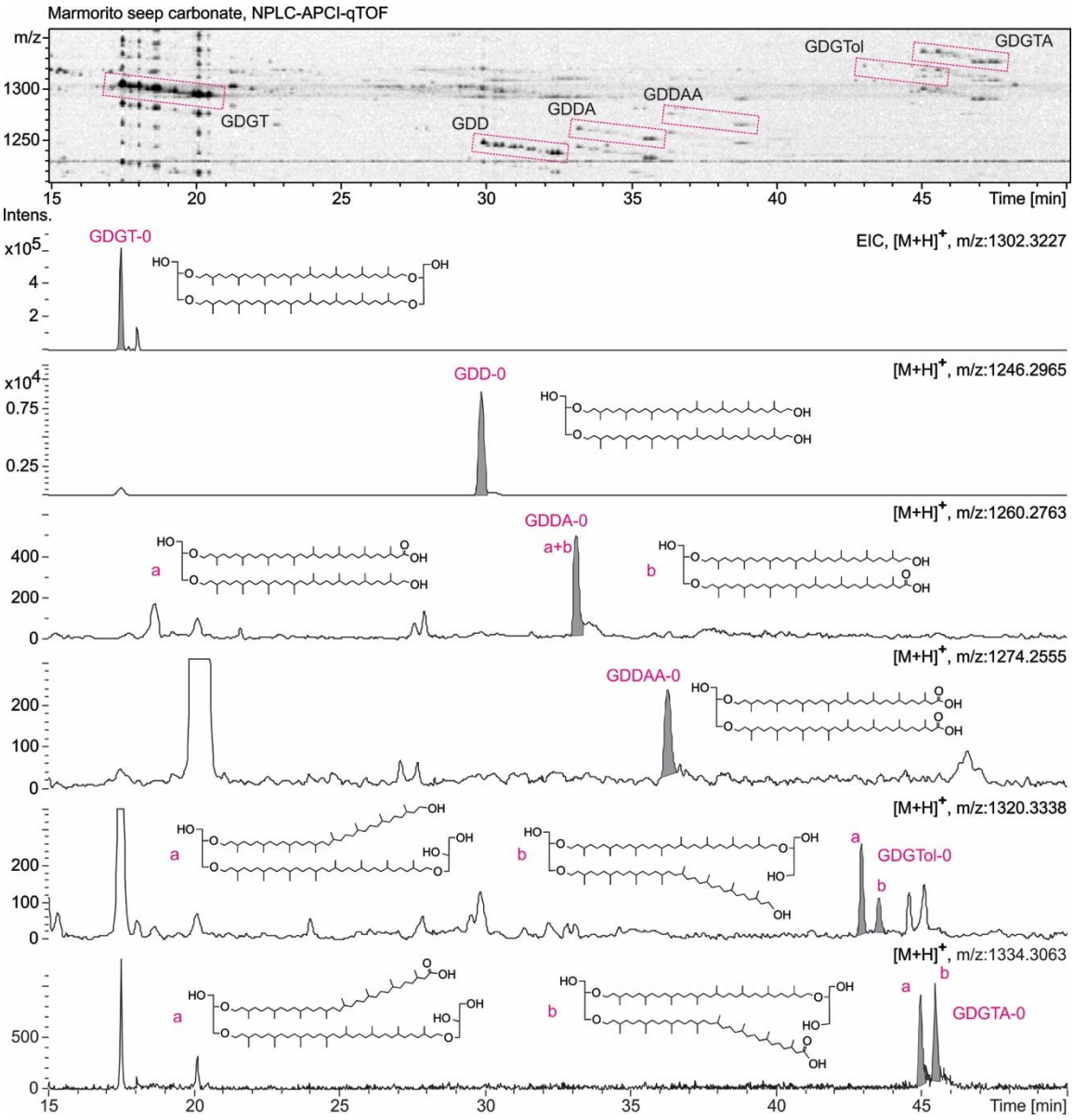

Fig. 1a

Density maps and extracted ion chromatograms (EICs) of NPLC-APCI-qTOF showing the detection of isoprenoidal GDGT-0 and its hydroxylated and carboxylated derivatives with two (Fig. 1a) or one biphytane units (Fig. 1b) in the Marmorito seep carbonate. Multiple isomers were observed for GDDA, GDGTol, GDGTA, GMM and GMGD and are labeled as 'a' and 'b'. The isomeric composition of GMGD, 'a' and 'b', may provide insights regarding the regioisomerism of GDGTs and will be subject of a future report.

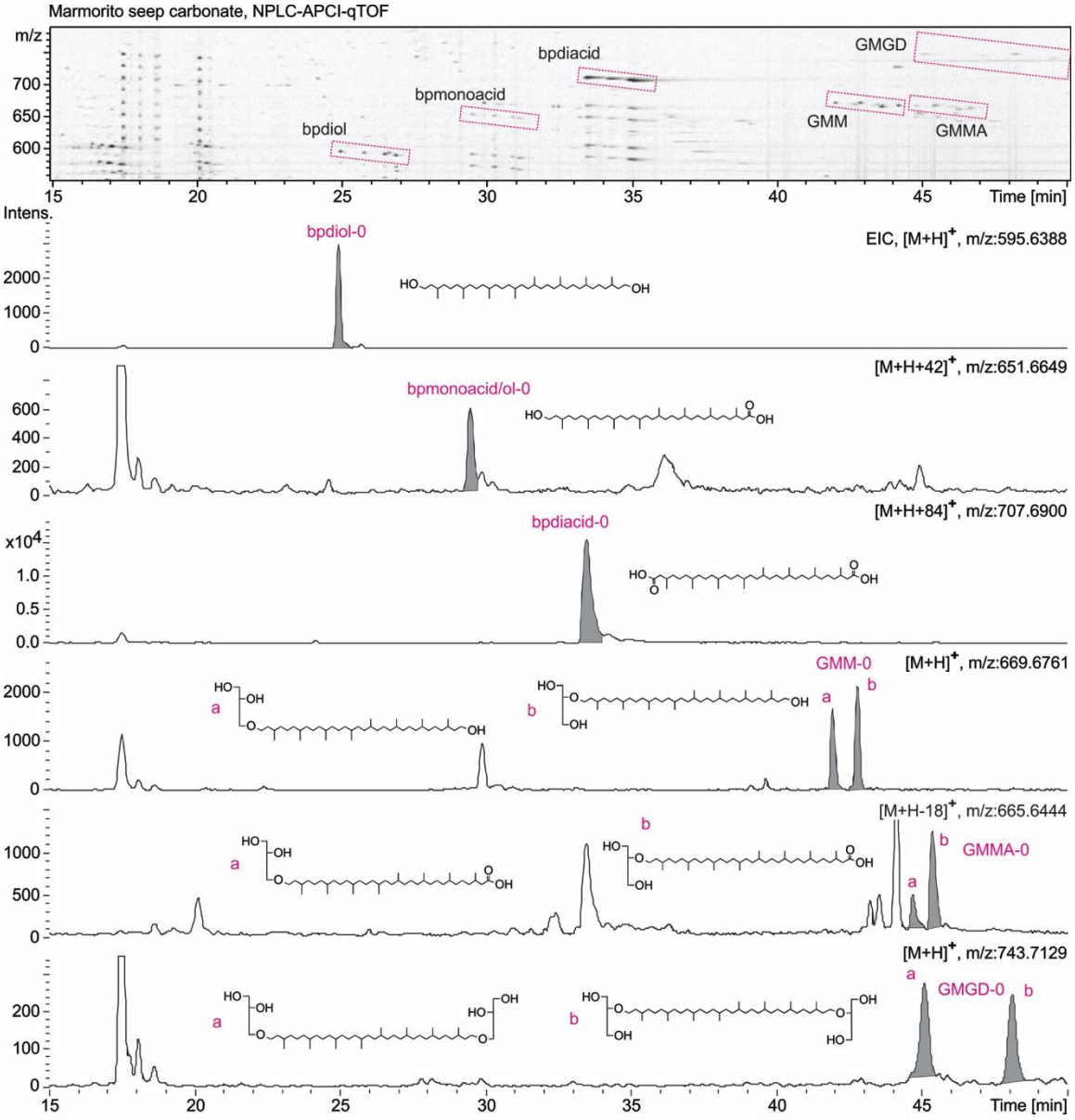

Fig. 1b

Density maps and EICs of NPLC-APCI-qTOF showing the detection of isoprenoidal GDGT-0 and hydroxylated and carboxylated derivatives with two (Fig. 1a) or one, biphytane units (Fig. 1b) in the Marmorito seep carbonate. Multiple isomers were observed for GDDA, GDGTol, GDGTA, GMM and GMGD and are labeled as 'a' and 'b'. The isomeric composition of GMGD, 'a' and 'b', may provide insights regarding the regioisomerism of GDGTs.

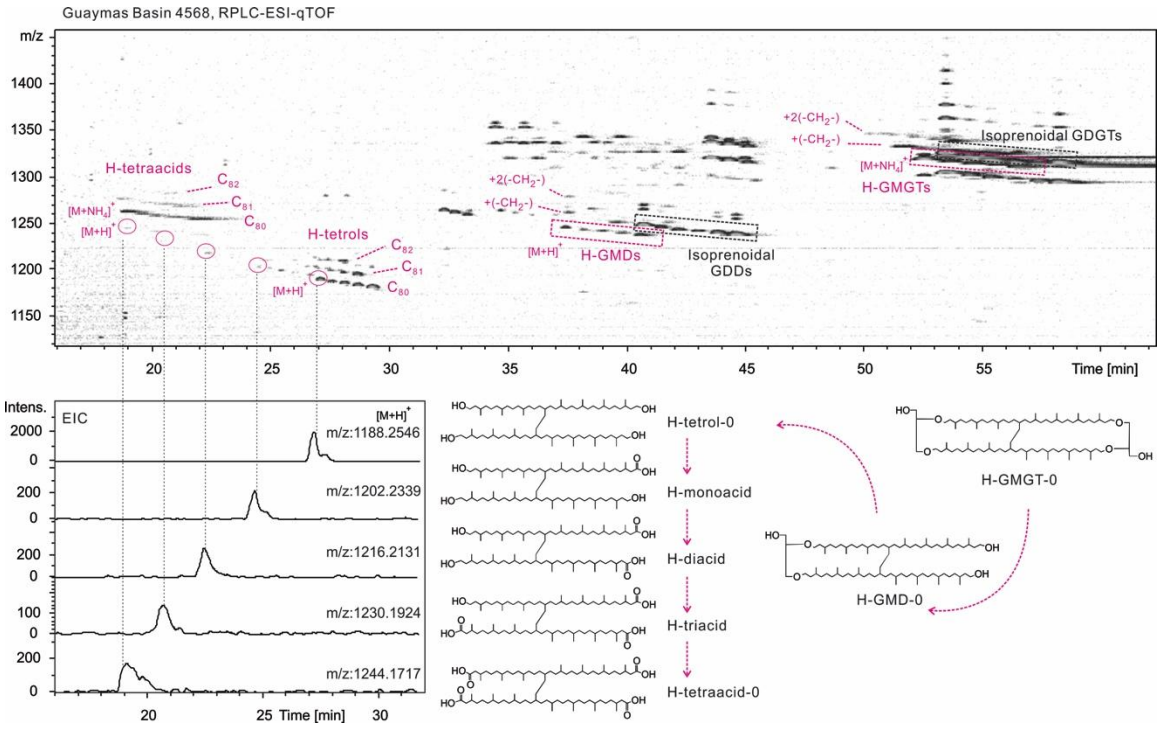

Fig. 2 Density maps and EICs derived from RPLC-ESI-qTOF analysis showing the detection of H-GMGTs and their hydroxylated and carboxylated derivatives in a hydrothermal sediment from the Guaymas Basin. Stepwise oxidation of the four hydroxyl groups in the H-tetrols possibly generated C_{80} mono-, di-, tri- and H-tetraacids. Mono- and di-methylated H-GMGTs, H-GMDs and corresponding C_{81}, C_{82} H-tetrols and H-tetraacids were also detected. Molecular structures of the intermediates are suggested. Isomers of monoacid, diacid and triacid may exist but could not be separated with the present LC methods.

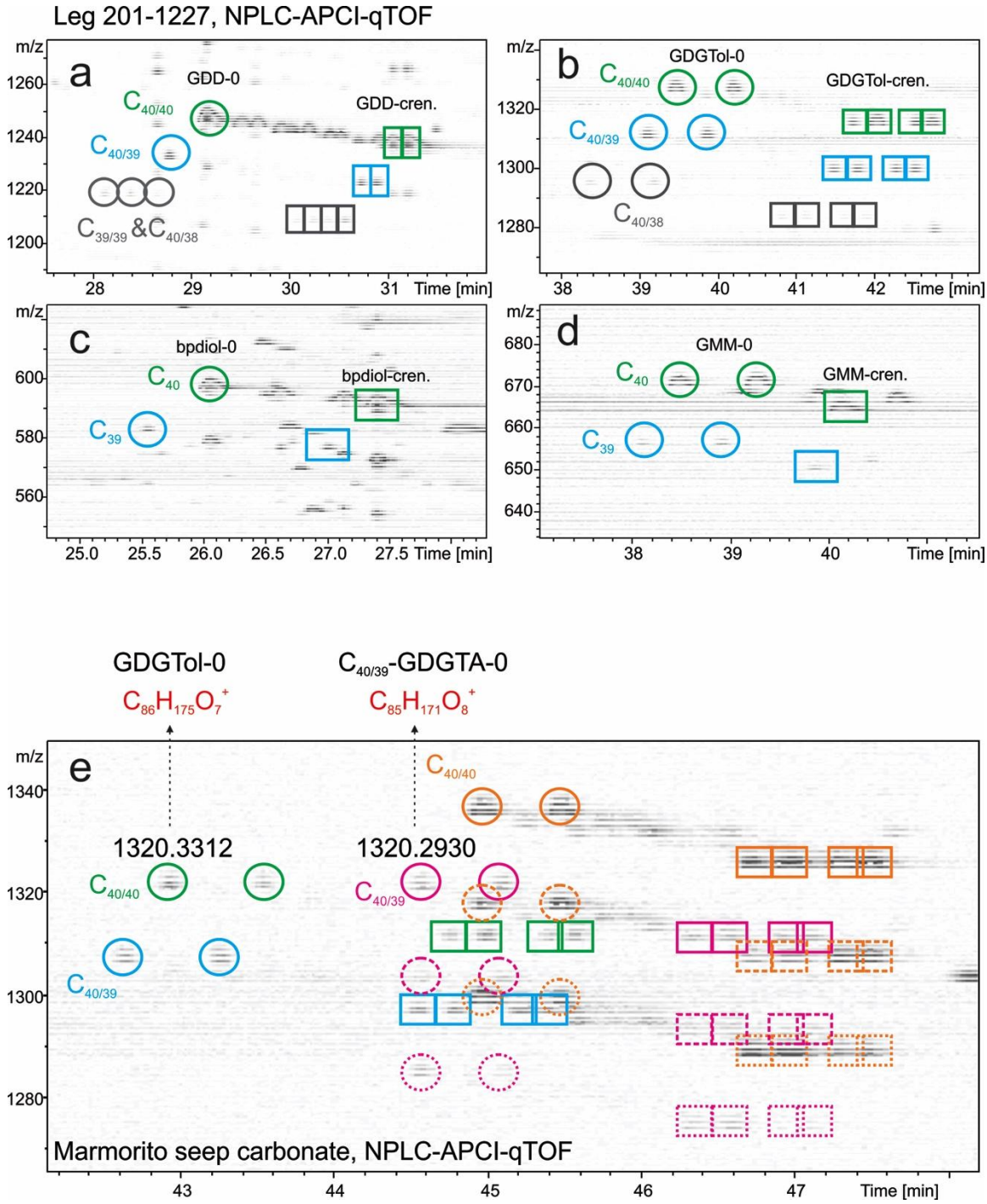

Fig. 3 Density maps of NPLC-APCI-qTOF showing in one marine sediment (Leg 201-1227) the detection of GDD, GDGTol, biphytane diol, GMM and their co-occurring further degradation derivatives with C_{39} and C_{38} based isoprenoids, (a-d). Highlighted are the most dominant components including the GDGT-0 (open circle) and crenarchaeol-related (rectangle) compounds. Different compound classes are also color coded. C_{40}

775 hydroxyl derivatives are in green, C_{39} in blue and the C_{38} related in grey, C_{40} carboxyl
776 derivatives are in orange and C_{39} in pink. Multiple isomers occur due to different ether
777 bonding and ring arrangements. The occurrence of $C_{40/39}$-GDGTA was shown in one
778 sample of Marmorito seep carbonate (e). The molecular ion of $C_{40/39}$-GDGTA-0 and
779 GDGTol-0 gives similar but distinguishable masses, m/z: 1320.2930 and 1320.3312,
780 respectively. Under APCI, dehydrated ions of carboxyl derivatives occurred (highlighted
781 ions with dashed lines).

782

783

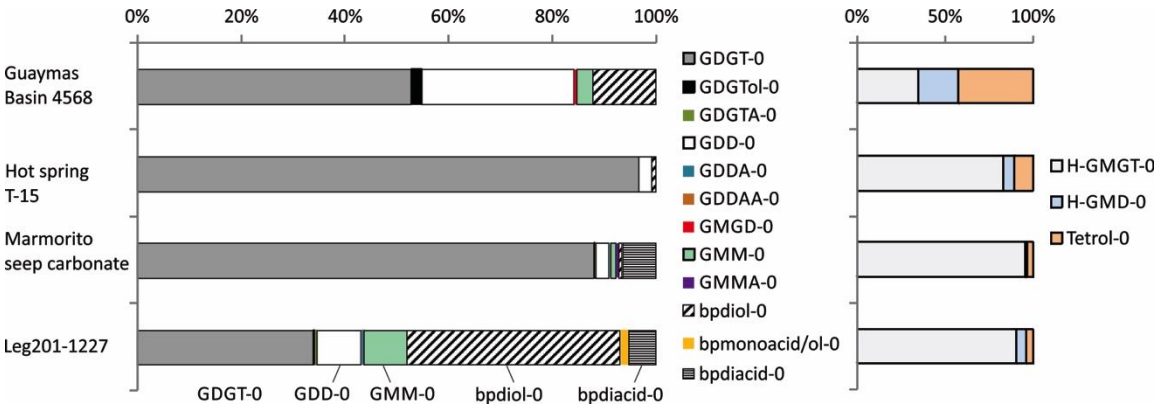

784

785

786 Fig. 4 Relative abundances of diagenetic derivatives of GDGT-0 (left panel) and H-
787 GMGT-0 (right panel) in four representative environmental samples.

788

789

790

791

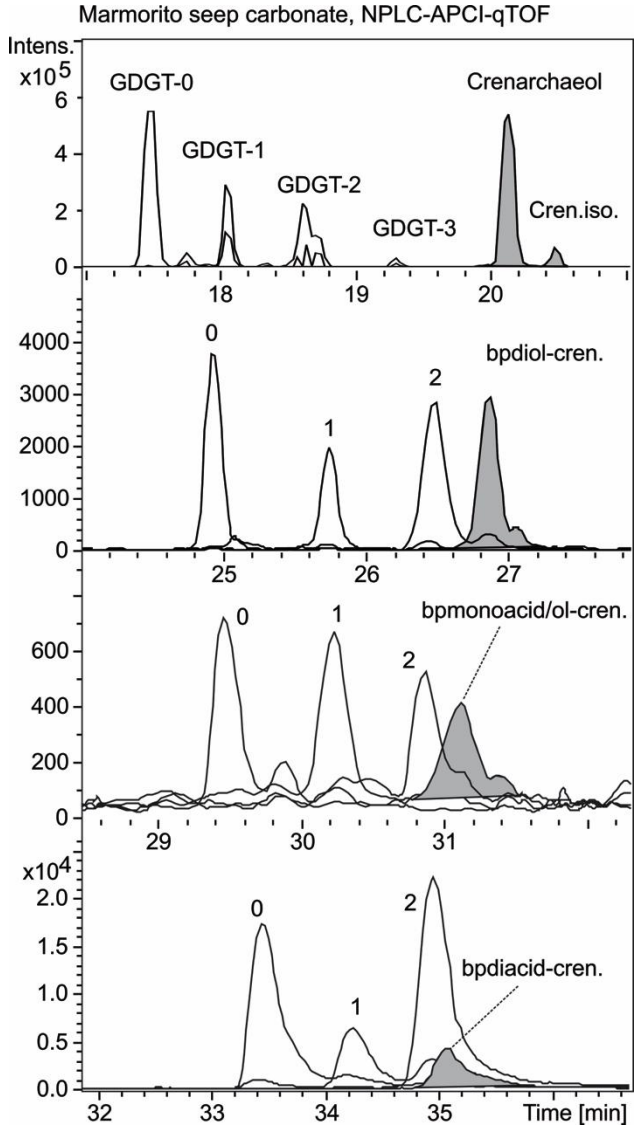

Fig. 5 Extracted ion chromatograms from NPLC-APCI-qTOF analysis, showing the distribution of GDGT, bpdiol, bpmonoacid/ol and bpdiacids in a seep carbonate, Marmorito. Peaks of crenarchaeol and its related derivatives are shaded; crenarchaeol derivatives have decreased abundances in the acid fractions.

798

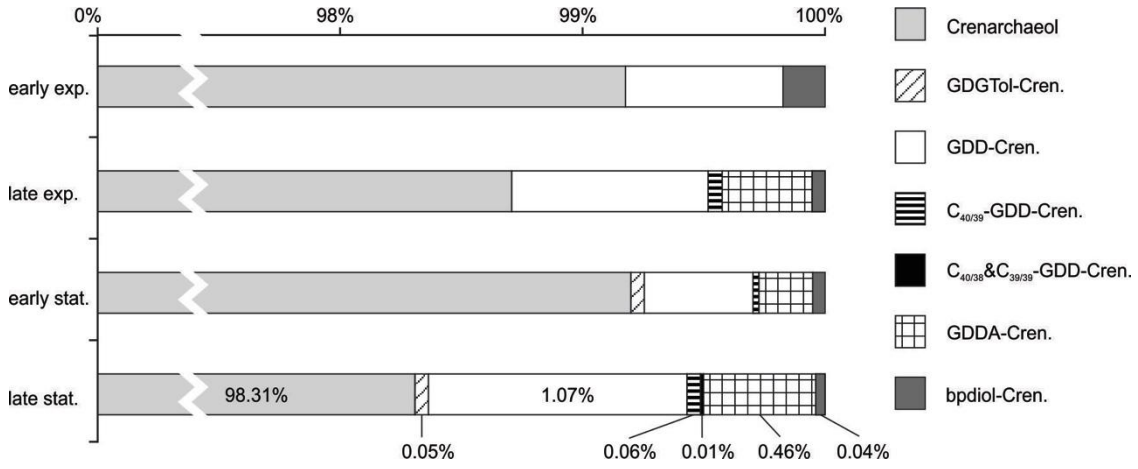

799

800

801

802 Fig. 6 The relative abundance of core crenarchaeol and its related hydroxyl, carboxyl and

803 C_{39} and C_{38} based derivatives in different growth phases of *N*. *maritimus*.

804

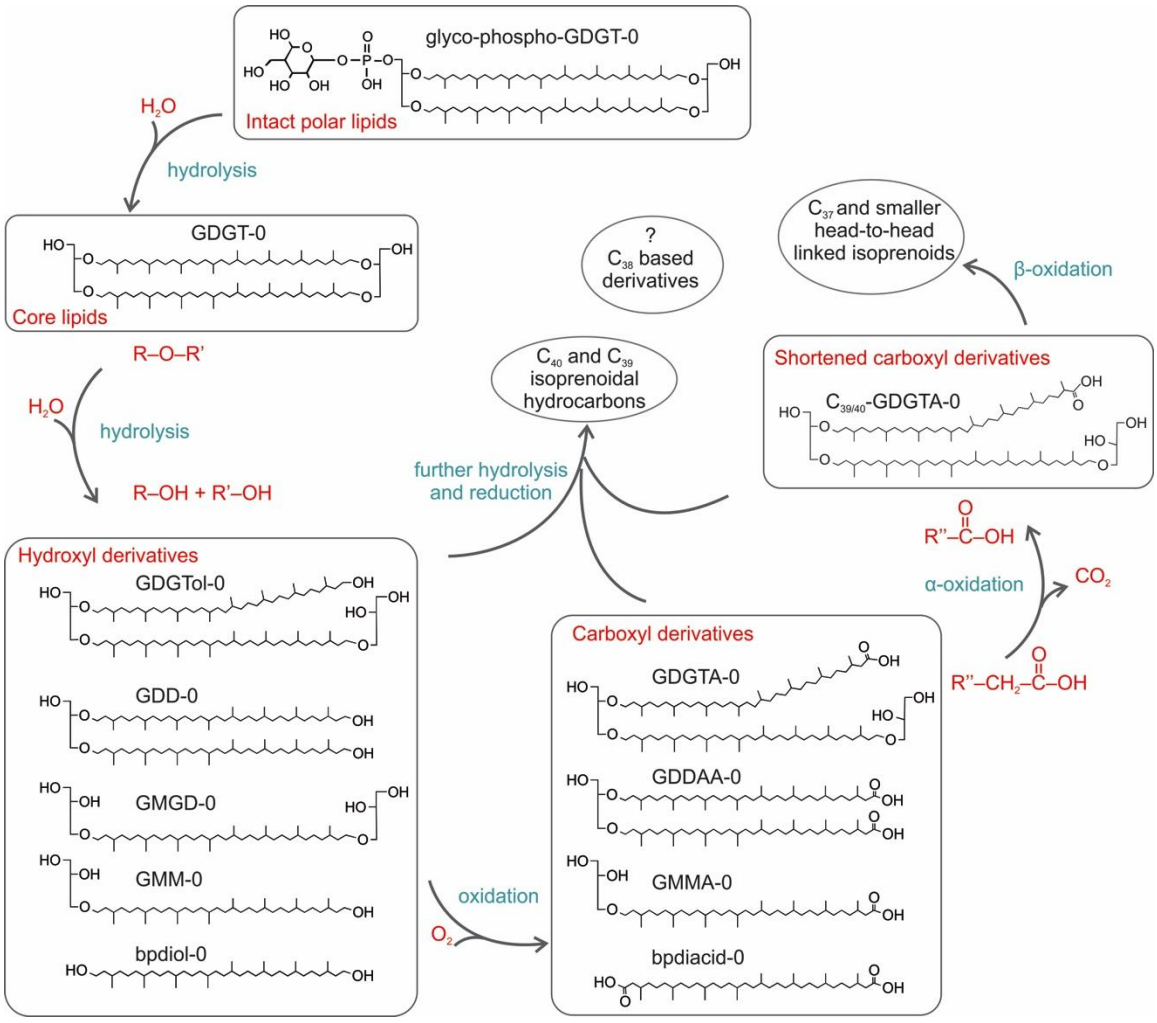

Fig. 7 Hypothetical scheme showing the suggested diagenetic pathways of GDGTs. GDGT-0 and its related IPL and degradation derivatives are used as an example. In the flow chart, R, R' and R'' represent different alkyl chains. Intermediate components, such as GDDA, bpmonoacid/ol are not included. The formation of C_{38} based isoprenoids is not clear and thus is labeled with '?'.

Supplementary information

Sample preparation

1. **Hot spring sediment T-15**

Sediment was collected from the bottom of a geothermal well located in Ruidian (Jinze hot spring: N 25.44138°, E98.46004°, Elevation:1740m. Tengchong County, Yunnan Province, China), with water pH of 6.71 and temperature of 80.6 °C. Roughly 5 g of freeze-dried sediment was extracted in an ultrasonic bath with methanol (MeOH; twice), methanol-dichloromethane (DCM; 1:1, v/v; twice) and finally DCM (twice). All supernatants were collected in a flask and completely dried under N_2. The total lipid extract was fractionated over a pre-activated silica gel chromatography into apolar (alkane) and polar (intact polar GDGTs and GDGT core lipids) fractions using *n*-hexane-DCM (9:1, v/v) and DCM-MeOH (1:1, v/v) as eluents respectively. The polar fraction was used for the lipid analysis in this study.

2. H-tetrol standards

An oilfield calcium naphthenate deposit was Soxhlet extracted sequentially (dichloromethane/*n*-hexane, 1/1, v/v, 300 mL, 8h; toluene/acetone, 3/2, v/v, 250 mL, 6h; propan-2-ol/dichloromethane, 4/1, v/v, 250mL, 6h) to remove interstitial oil and the residue dried (overnight, 70˚C) before acidification by heating (70˚C, overnight) in a capped and sealed vial with hydrochloric acid (3 mL) and cyclohexane (3 mL). The acidified organic fraction was recovered by extraction into diethylether (DEE; 3 x 5 mL) by mixing (vortex 10 s) and centrifugation (2500 rpm/3 min). Solvent was removed from

838 the decanted supernatant under blow-down (N_2, 70˚C) prior to dilution in DEE/0.1%
839 ammonia (8 mL), loading on a pre-conditioned (1% aqueous ammonia, 20 mL; water, 20
840 mL; DEE, 10 mL) SAX solid phase extraction cartridge (Sigma-Aldrich Company Ltd.,
841 Dorset, UK; DSC-SAX, 12 mL, 2 g) and sequentially eluting the cartridge with 20 mL
842 volumes of DEE, dichloromethane and DEE/2% formic acid (FA). Solvent was removed
843 from the DEE/2% FA fraction ('acid fraction') under blow-down (N_2, 70˚C) and an
844 aliquot per-trimethylsilylated with BSTFA/1% TMCS (Sigma-Aldrich Company Ltd.,
845 UK; ca. 50 µL, 70˚C, 1 hr) before dilution in cyclohexane for analysis using high
846 temperature gas chromatography (HTGC; Fig. SX1), or per-methylation for infusion
847 electrospray ionization/mass spectrometry (ESI-MS; Fig. SX2). An aliquot of the isolated
848 acid fraction was diluted in DEE for infrared spectroscopy (Fig. SX3).
849
850 The isolated acid fraction was reduced to alcohols by treatment with lithium aluminum
851 hydride ($LithAlH_4$; Sigma-Aldrich Company Ltd., UK; 1M in DEE). Dried acid fraction
852 was dissolved in a small volume (ca. 1 mL) dry DEE (sodium wire) and transferred with
853 washings to a small three-neck flask with Teflon flea and fitted with a Subaseal, calcium
854 chloride drying tube condenser and a glass stopper, all over a magnetic stirring block.
855 $LithAlH_4$ solution (ca. 3 mL) was pumped into the flask under nitrogen through the
856 Subaseal whilst stirring, additional dry DEE (ca. 5mL) was added through the condenser
857 to break up formed solids, before placing a bowl of warm water under the flask for 10
858 minutes. After the reaction vessel had cooled, wet DEE (prepared by mixing DEE and
859 water in separating funnel and drawing off aqueous phase) was added (10 mL, drop-wise
860 at first) to hydrolyse unreacted hydrides, followed by drop-wise addition of sulphuric

861 acid (10% aqueous; ca. 1 mL) to destroy remaining $LithAlH_4$. The contents of the flask
862 were transferred with washings (ca. 3 mL, 10% $H_2SO_{4(aq)}$) to a separating funnel and the
863 organic phase ('alcohol fraction') collected after washing with water (3 x 3 mL). Solvent
864 was removed from the alcohol fraction by blow-down (N_2, 70˚C) and aliquots prepared
865 for HTGC, ESI-MS and IR spectroscopy as above. All solvents were HPLC grade
866 (Rathburn Chemicals Ltd., Walkerburn, UK or Fisher Scientific UK Ltd., Loughborough,
867 UK) or LC/MS grade (Chromasolv®; Sigma-Aldrich Company Ltd., Dorset, UK), water
868 was Elga Maxima (18.2 mΩ; Elga Ltd., Buckinghamshire, UK).
869
870 Reduction of the tetraacids to tetrols was monitored using HTGC (Fig. SX1), ESI-MS
871 (Fig. SX4 and SX5) and IR spectroscopy (Fig. SX3). The HTGC system comprised an
872 Agilent 6890 GC fitted with cool-on-column inlet (+3˚C track oven mode; 0.5 µL manual
873 injection), flame ionization detector (435˚C) and Varian VF-5ht Ultimetal column (15 m
874 x 0.25 mm x 0.1 µm) with helium carrier gas (1 ml min^{-1}, constant flow) and oven
875 programme from 40 – 430˚C at 10˚C min^{-1} with 10 min hold.
876
877 Infusion ESI-MS was carried out in positive ionization mode using a Finnigan Mat
878 LCQ™ (ThermoFinnigan, San Jose, CA, USA) with ESI interface. Samples were diluted
879 in propan-2-ol/10mM ammonium acetate and infused at 3 µL min^{-1} with a Hamilton
880 (Reno, CA, USA) 1725N (250 µL) syringe using the built-in syringe pump. Mass spectral
881 data were acquired (and averaged over 1 minute) and processed using Xcalibur software.
882 Typical instrument parameters were: source voltage (±) 4.5 kV; capillary voltage (±) 60
883 V; capillary temperature 200 °C; nitrogen sheath gas flow rate 24 (arbitrary units).

884 Instrumental parameters were optimised on the most abundant ion using the autotune
885 function.
886
887 Infrared spectroscopy was carried out using a Bruker Alpha Platinum ATR (Bruker Optik
888 GmbH, Ettlingen, Germany) by measuring 32 sample scans (resolution 4 cm^{-1};
889 transmittance) and recording data between 4000 – 375 cm^{-1}. Background comprised 32
890 scans without sample.
891

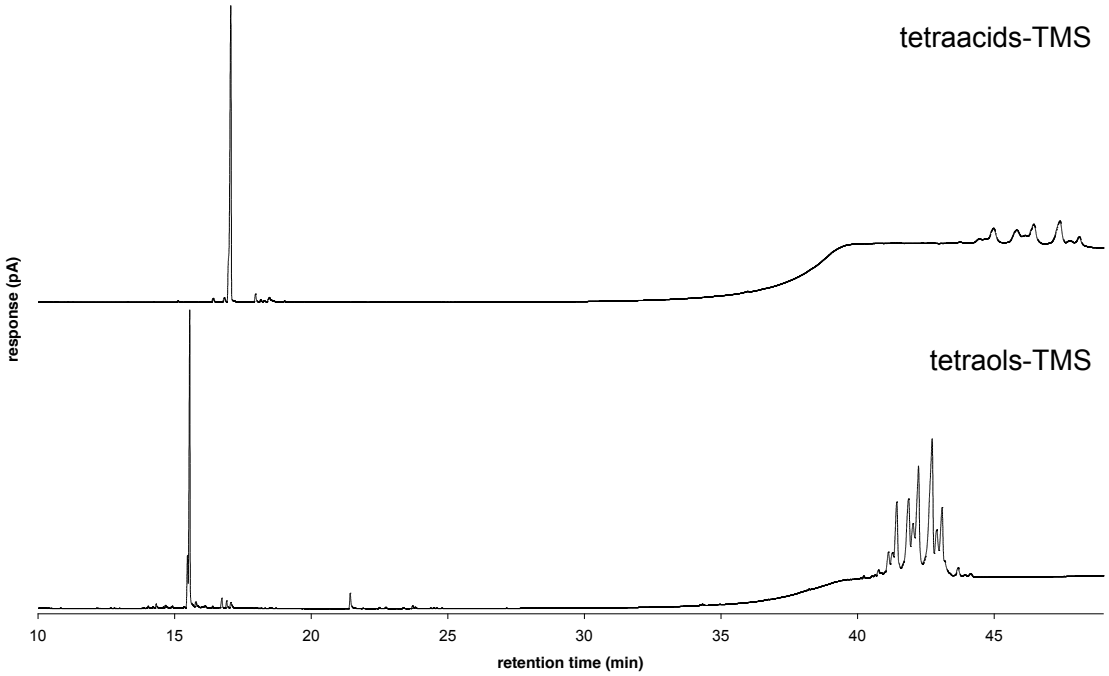

892
893 Figure SX1. High temperature gas chromatograms of trimethylsilylated tetraacids
894 obtained from an oilfield deposit (upper) and lower the trimethylsilylated tetraols
895 obtained following $LithAlH_4$ reduction (lower).
896

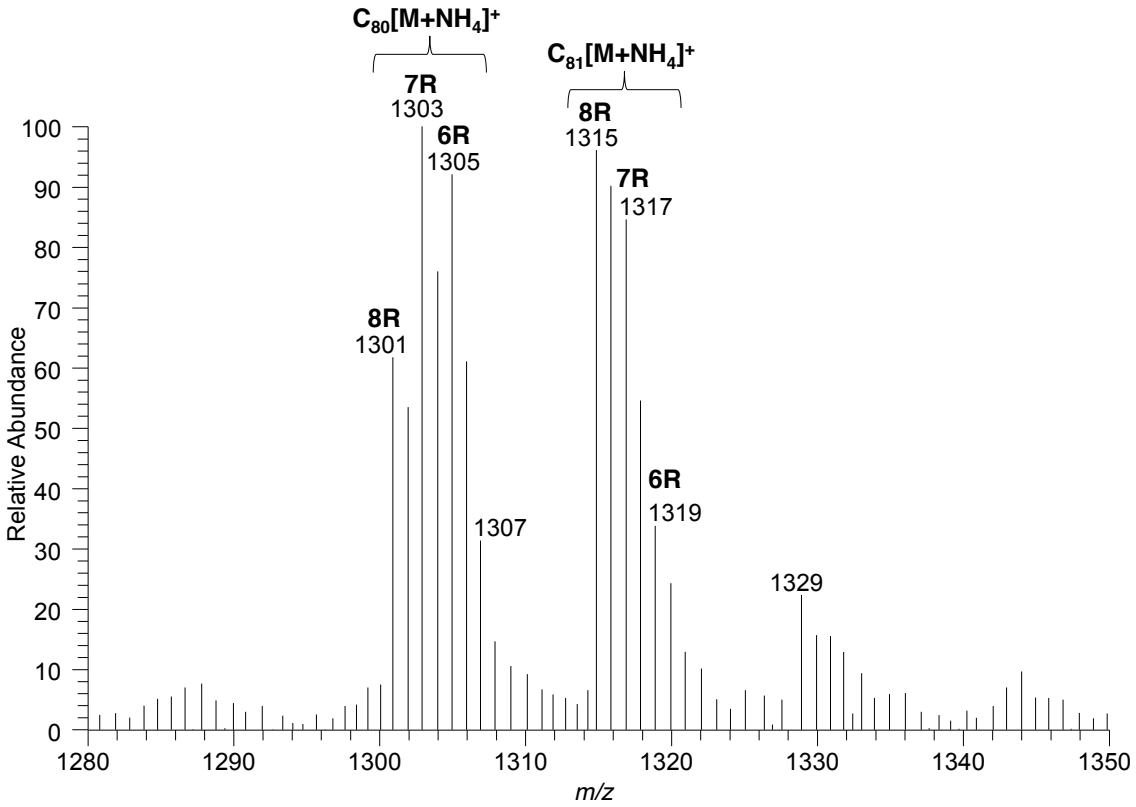

897

898 Figure SX2. Averaged mass spectrum (18.6 – 19.6 min) from Infusion ESI-MS of per-

899 methylated esters of tetraacids obtained from an oilfield deposit (nR refers to the number

900 of cyclopentyl rings in the molecule).

901

902

903

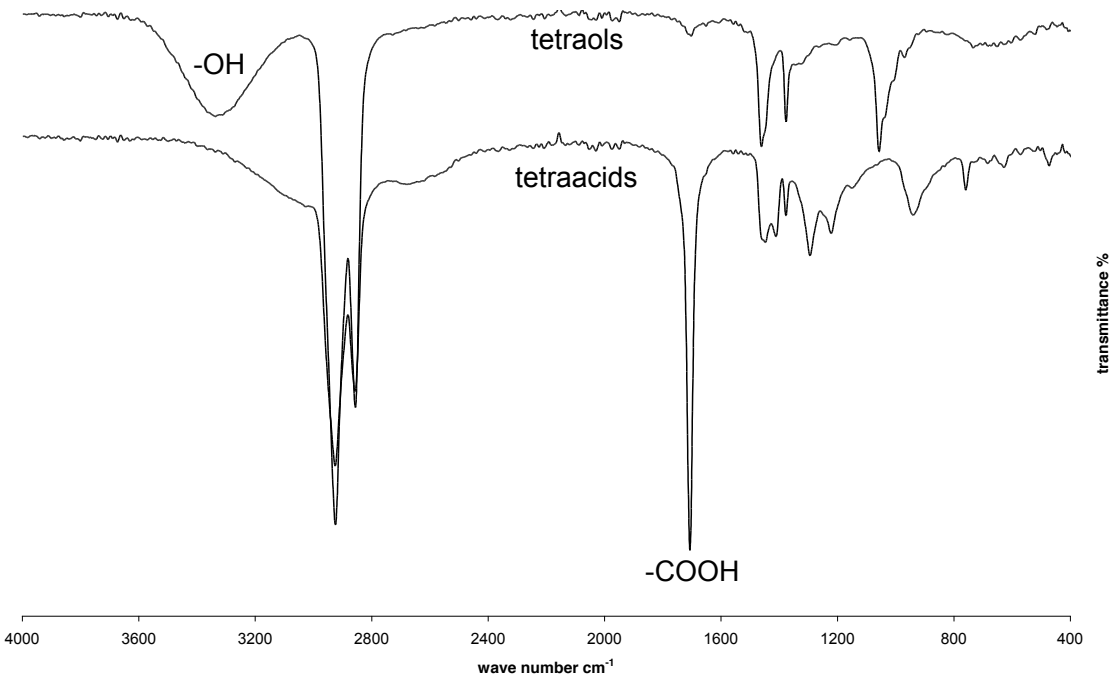

904

905 Figure SX3. FTIR transmittance spectra of tetraacids isolated from an oilfield deposit

906 (lower) and tetraols produced from the tetraacids by $LithAlH_4$ reduction (upper).

907

908

909

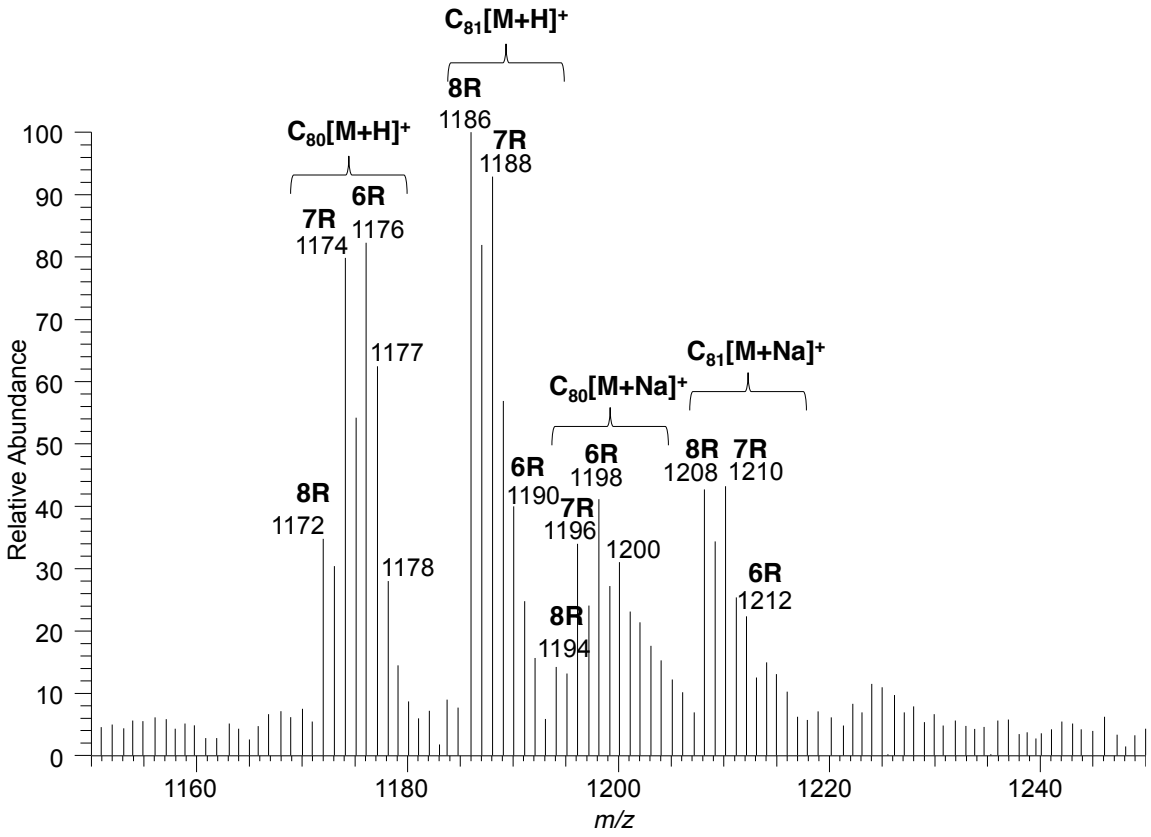

910

911 Figure SX4. Infusion ESI-MS of underivatised tetraols obtained from the LithAl

912 reduction of tetraacids from an oilfield deposit (nR refers to the number of cyclopentyl

913 rings in the molecule).

914

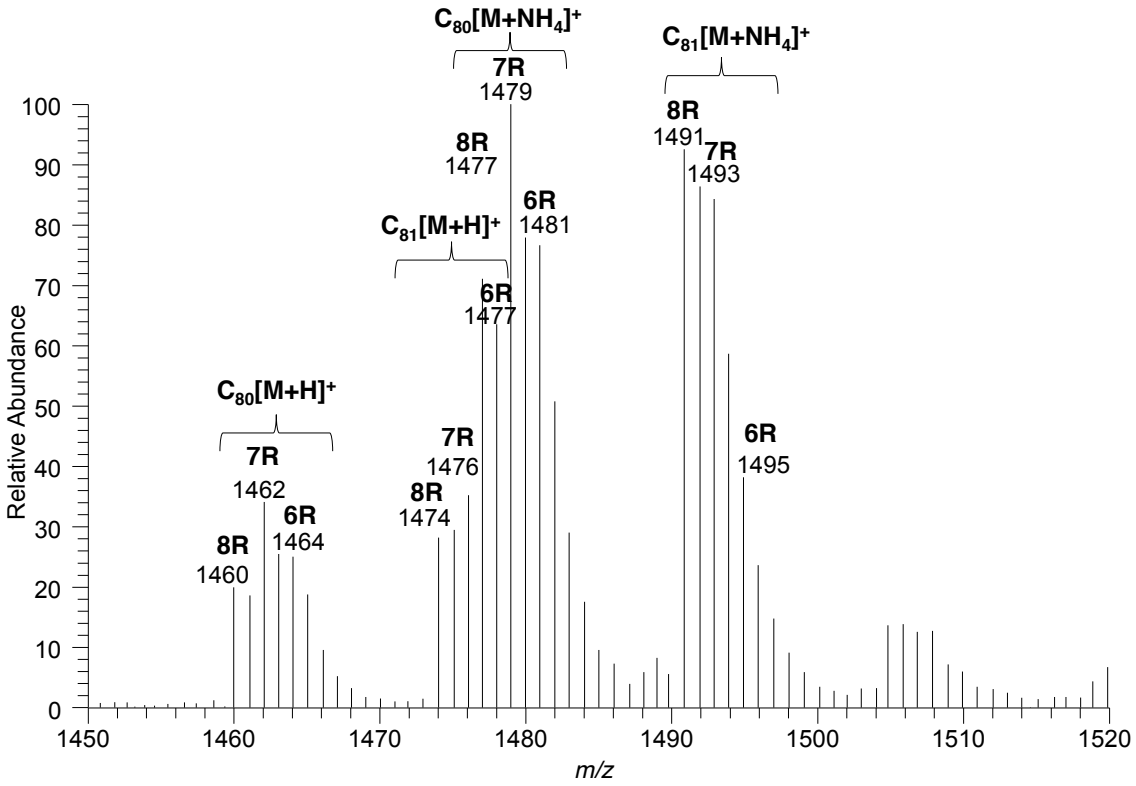

Figure SX5. Infusion electrospray ionization (+ve) mass spectrum of per-trimethylsilylated tetraols obtained from the LithAl reduction of tetraacids from an oilfield deposit (nR refers to the number of cyclopentyl rings in the molecule).

3. Acid hydrolysis of GDGT-0 standard

GDGT-0 standard was isolated with a semi-preparative LC protocol (as described in Zhu et al., 2014) from acid-hydrolyzed biomass of *Archaeoglobus fulgidus*. Strong acid hydrolysis was then performed with 10% methanolic HCl and GDGT-0 standard under 70 °C for 96 hours. After dried with a N_2 flow the treated sample was dissolved in *n*-hexane for NPLC-APCI-MS analysis.

928

929 **Reference:**

930 Zhu, C., Meador, T.B., Dummann, W., Hinrichs, K.-U., 2014. Identification of unusual
931 butanetriol dialkyl glycerol tetraether and pentanetriol dialkyl glycerol tetraether lipids in
932 marine sediments. *Rapid Commun*. *Mass Spectrom*. 28, 332–338.

933

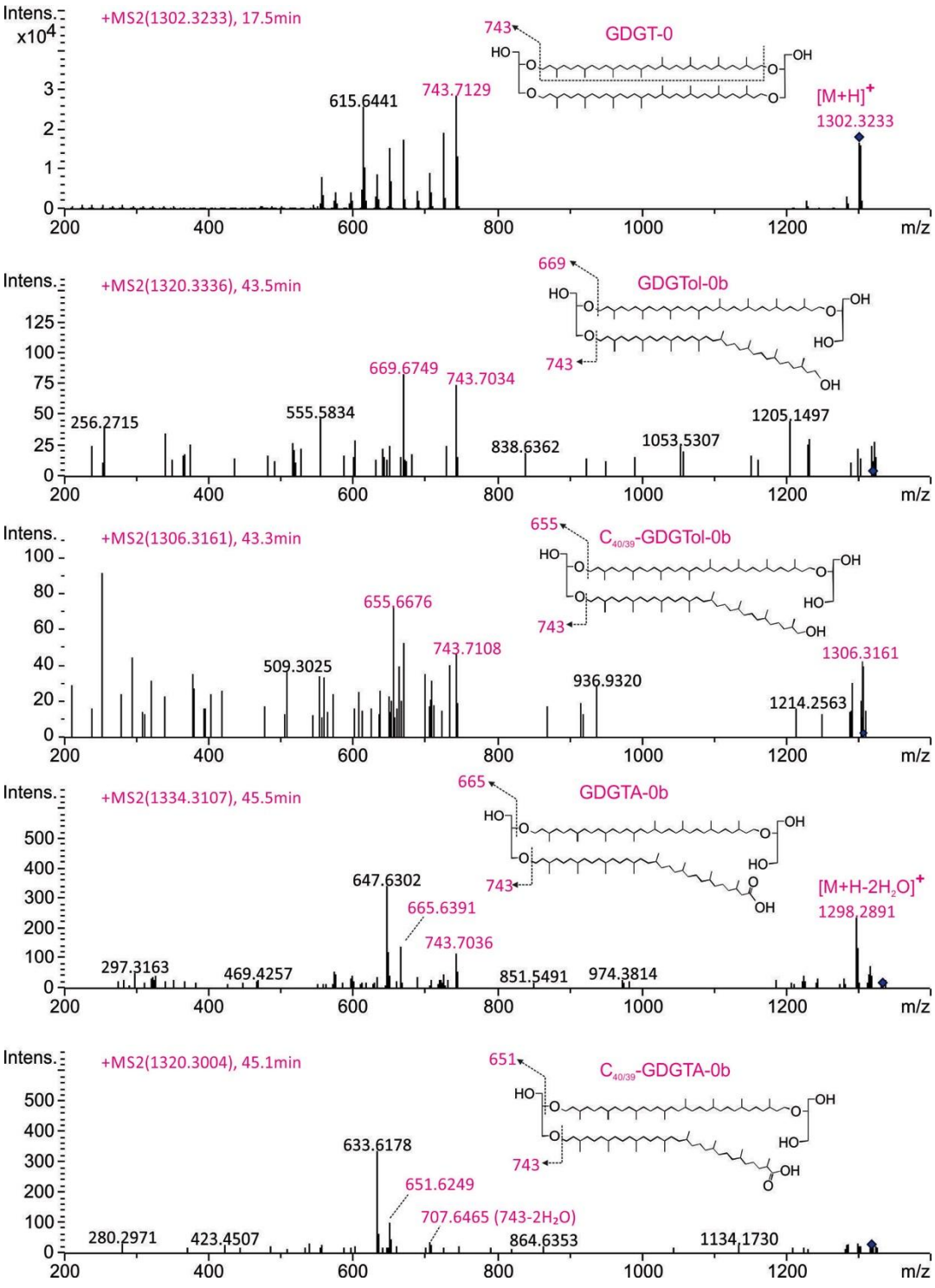

934

935

936 **Figure S1a.** MS^2 fragmentation patterns supporting the identification of GDGT-0,
937 GDGTol-0 and GDGTA-0 in Fig. 1a, and $C_{40/39}$-GDGTol-0 and $C_{40/39}$-GDGTA-0 in Fig.
938 3e.

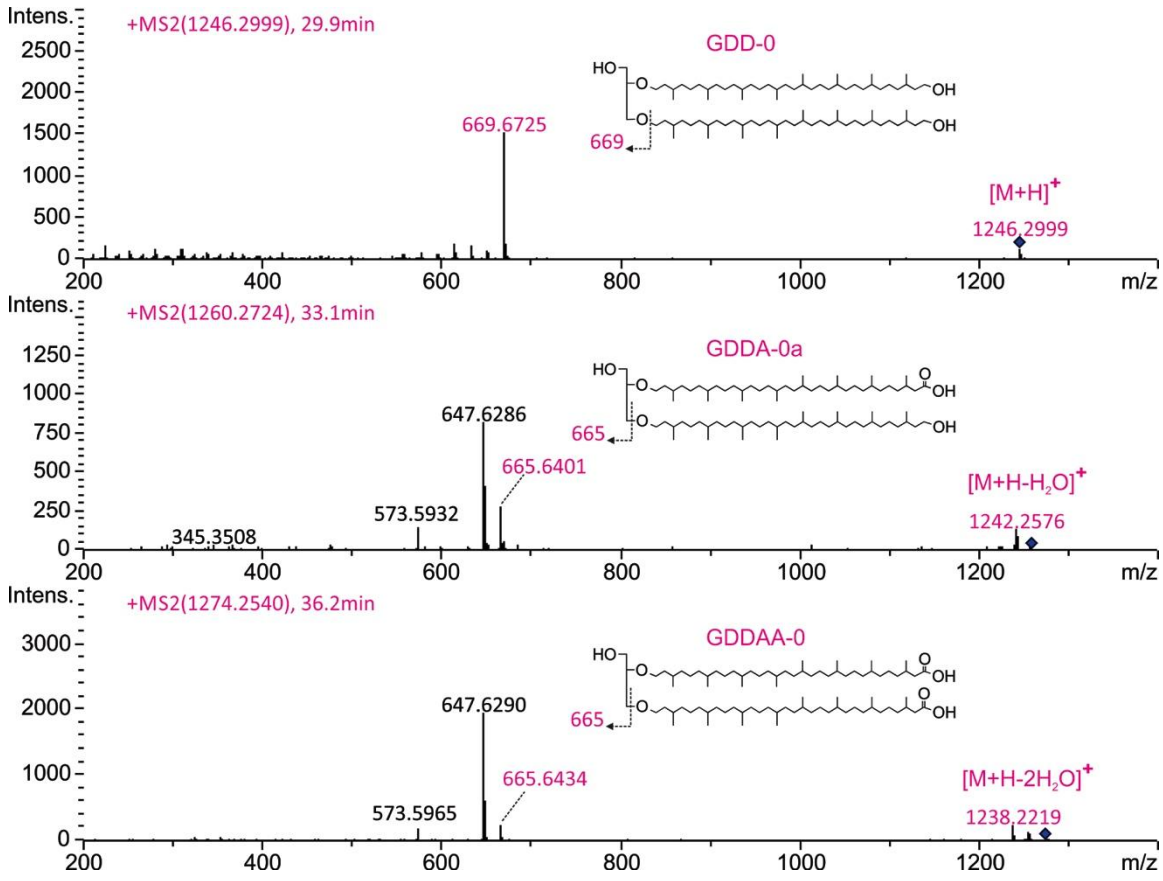

Figure S1b. MS^2 fragmentation patterns supporting the identification of GDD-0, GDDA-0 and GDDAA-0 in Fig. 1a**.**

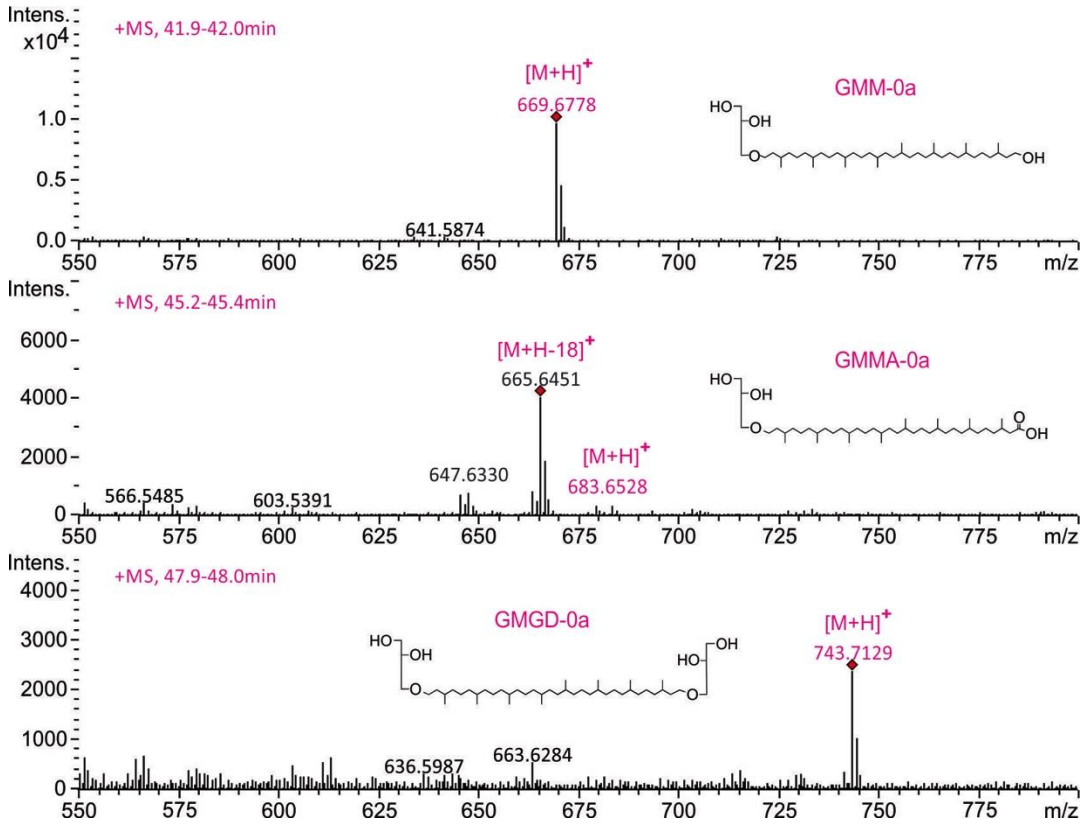

946

947

948 **Figure S1c.** MS[1] ions supporting the identification of GMM-0, GMMA-0 and GMGD-0
949 in Fig. 1b.

950

951

952

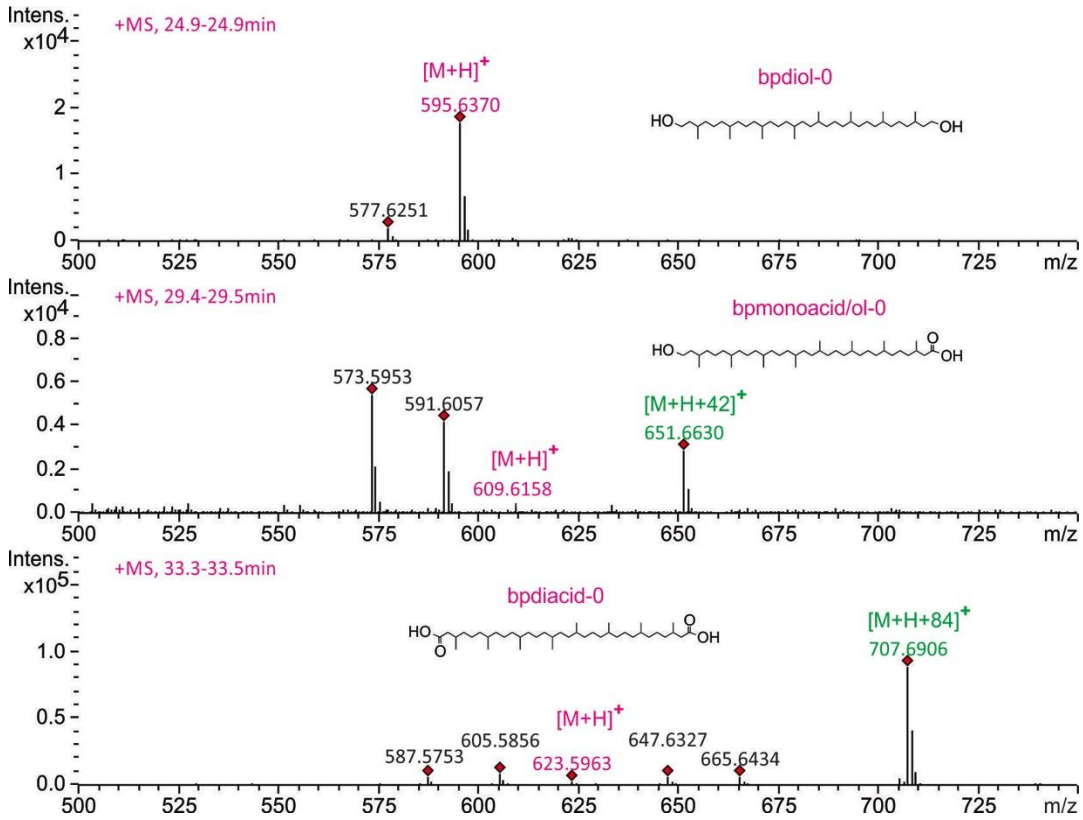

Figure S1d. MS^1 ions supporting the identification of bpdiol-0, bpmonoacid/ol-0 and bpdiacid-0 in Fig. 1b.

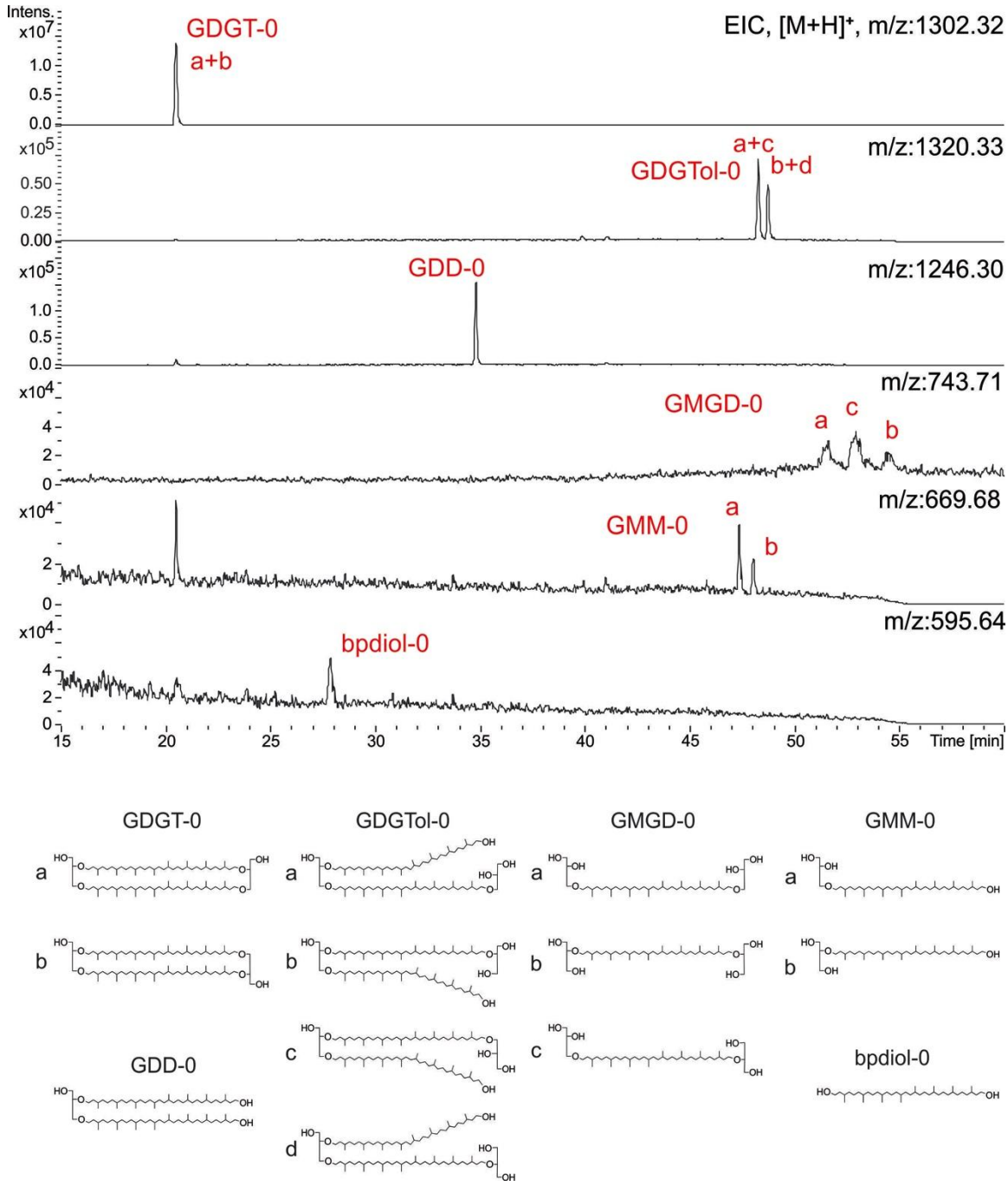

961

962

963 **Figure S2**

964 Major hydroxyl derivatives released from GDGT-0 by chemical degradation, a mild ether
965 cleavage conducted by adding 1000ng GDGT-0 into 1mL of 10% HCl in methanol, and

heated to 70 °C for 96 hours. The composition of GMGDs indicated a nearly 1:1 mixture of parallel and anti-parallel GDGT-0.

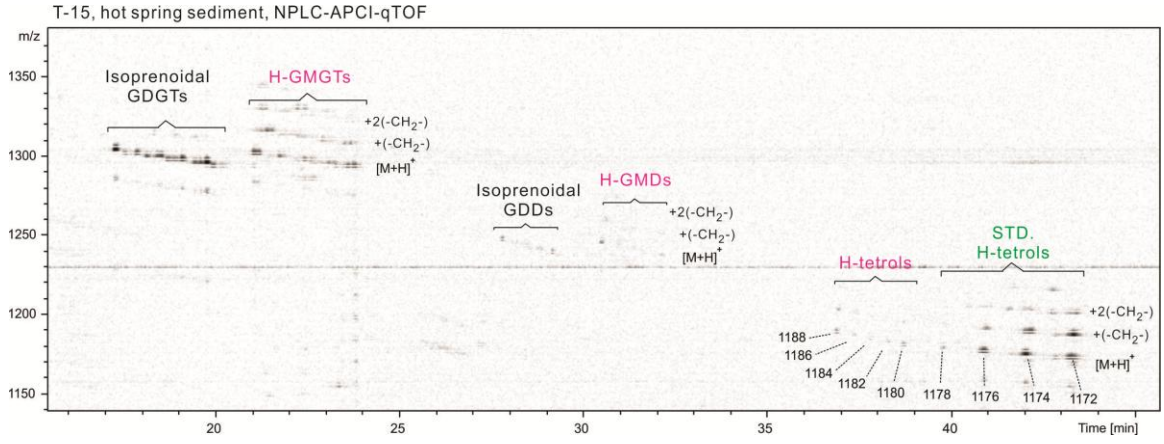

Figure S3

Density maps of NPLC-APCI-qTOF showing the occurrence of H-GMGTs and their degradation derivatives in the hot spring sediment, T-15. The identification of H-tetrols are confirmed by their similar chromatographic behavior with added standards (green color text).

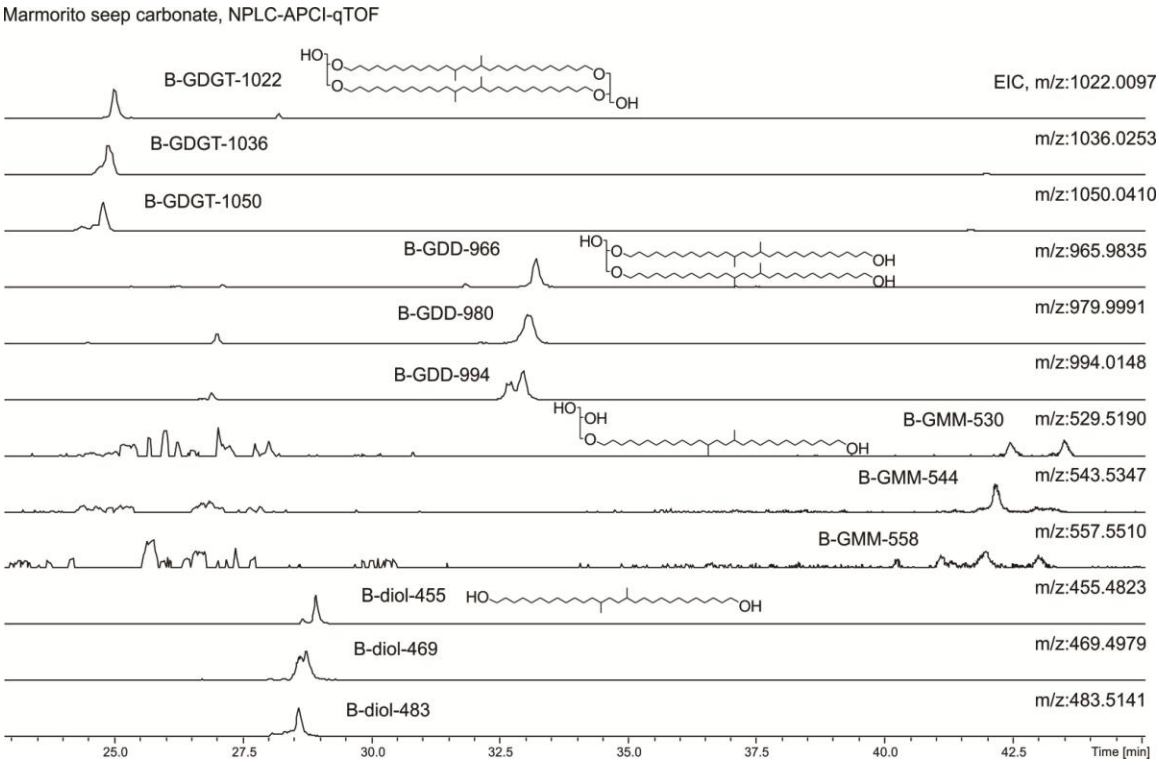

980

981 **Figure S4**

982 Extracted ion chromatograms of NPLC-APCI-qTOF showing the occurrence of branched
983 GDGTs and derivatives in Marmorito seep carbonate.

984

985

986

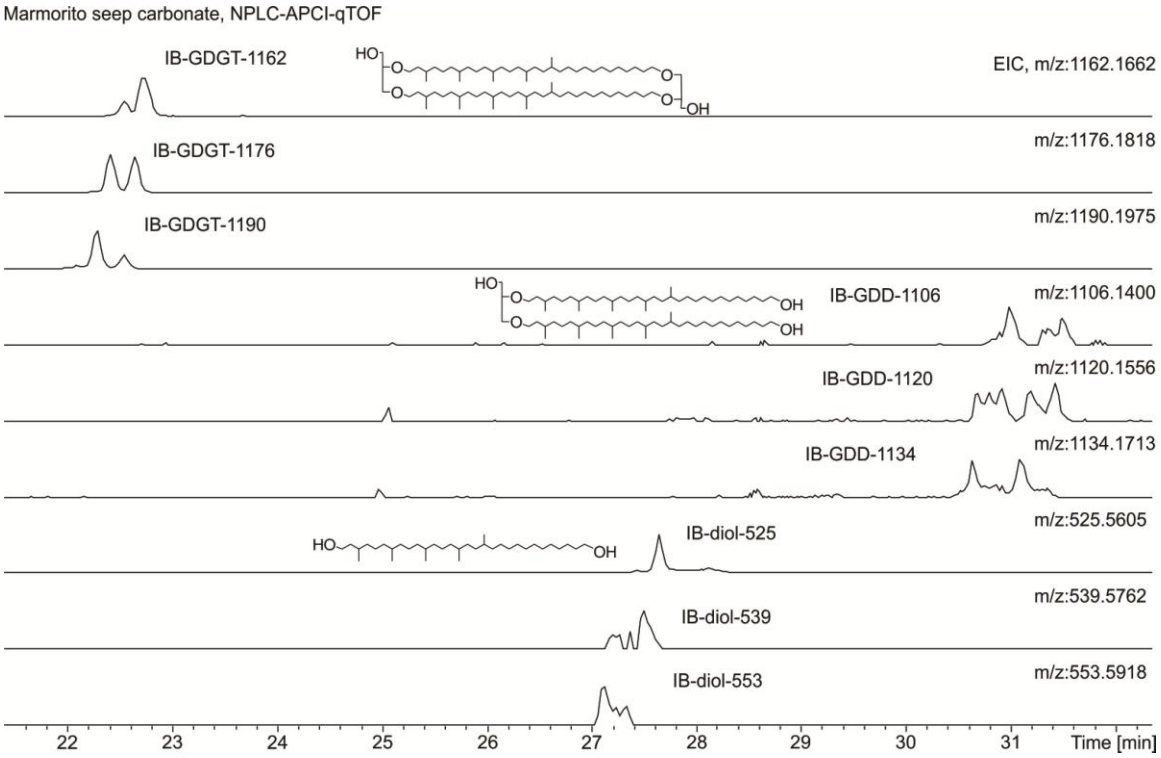

987

988 **Figure S5**

989 Extracted ion chromatograms of NPLC-APCI-qTOF showing the occurrence of IB-
990 GDGTs and derivatives in Marmorito seep carbonate.

991

Table

Compounds	Abbreviation	Structural illustration	Distribution				
			Leg201-1227	Marmorito seep carbonate	Guaymas Basin 4568	Hot spring T-15	*N. maritimus* late stat. phase
glycerol dialkyl glycerol tetraether	GDGT	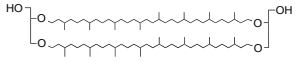	+	+	+	+	+
glycerol dialkyl glycerol triether alcohol	GDGTol	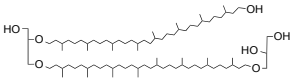	+	+	+	n.d.	+
glycerol dialkyl glycerol triether acid	GDGTA	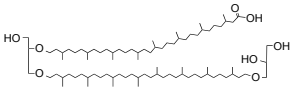	+	+	n.d.	n.d.	n.d.
glycerol dibiphytanol diether	GDD	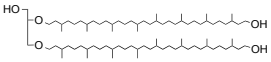	+	+	+	+	+
glycerol dibiphytanol diether monoacid	GDDA	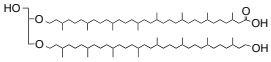	+	+	+	n.d.	+
glycerol dibiphytanol diether diacid	GDDAA	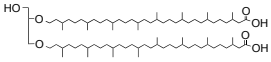	n.d.	+	n.d.	n.d.	n.d.
glycerol monobiphytanyl glycerol diether	GMGD	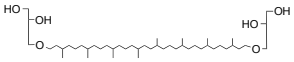	+	+	+	n.d.	n.d.
glycerol monobiphytanol monoether	GMM	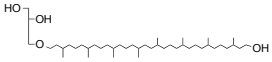	+	+	+	n.d.	n.d.
glycerol monobiphytanol monoether acid	GMMA	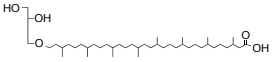	n.d.	+	n.d.	n.d.	n.d.
biphytanic diol	bpdiol	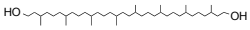	+	+	+	+	+
biphytanic monoacid	bpmonoacid/ol	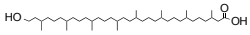	+	+	n.d.	n.d.	n.d.
biphytanic diacid	bpdiacid	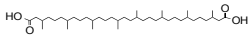	n.d.	+	n.d.	n.d.	n.d.
H-shaped glycerol monoalkyl glycerol tetraether	H-GMGT	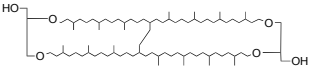	+	+	+	+	n.d.
H-shaped glycerol monoalkyl diether	H-GMD	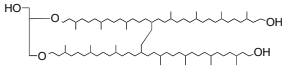	+	+	+	+	n.d.
H-shaped C_{80} tetrol	H-tetrol	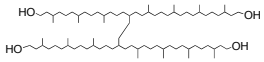	+	+	+	+	n.d.
H-shaped C_{80} monoacid	H-monoacid	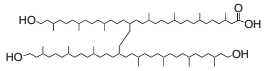	n.d.	n.d.	+	n.d.	n.d.
H-shaped C_{80} diacid	H-diacid	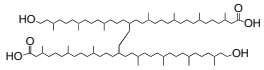	n.d.	n.d.	+	n.d.	n.d.
H-shaped C_{80} triacid	H-triacid	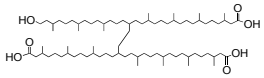	n.d.	n.d.	+	n.d.	n.d.
H-shaped C_{80} tetraacid	H-tetraacid	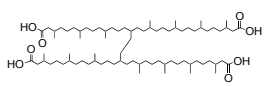	n.d.	n.d.	+	n.d.	n.d.

Figure

Click here to download high resolution image

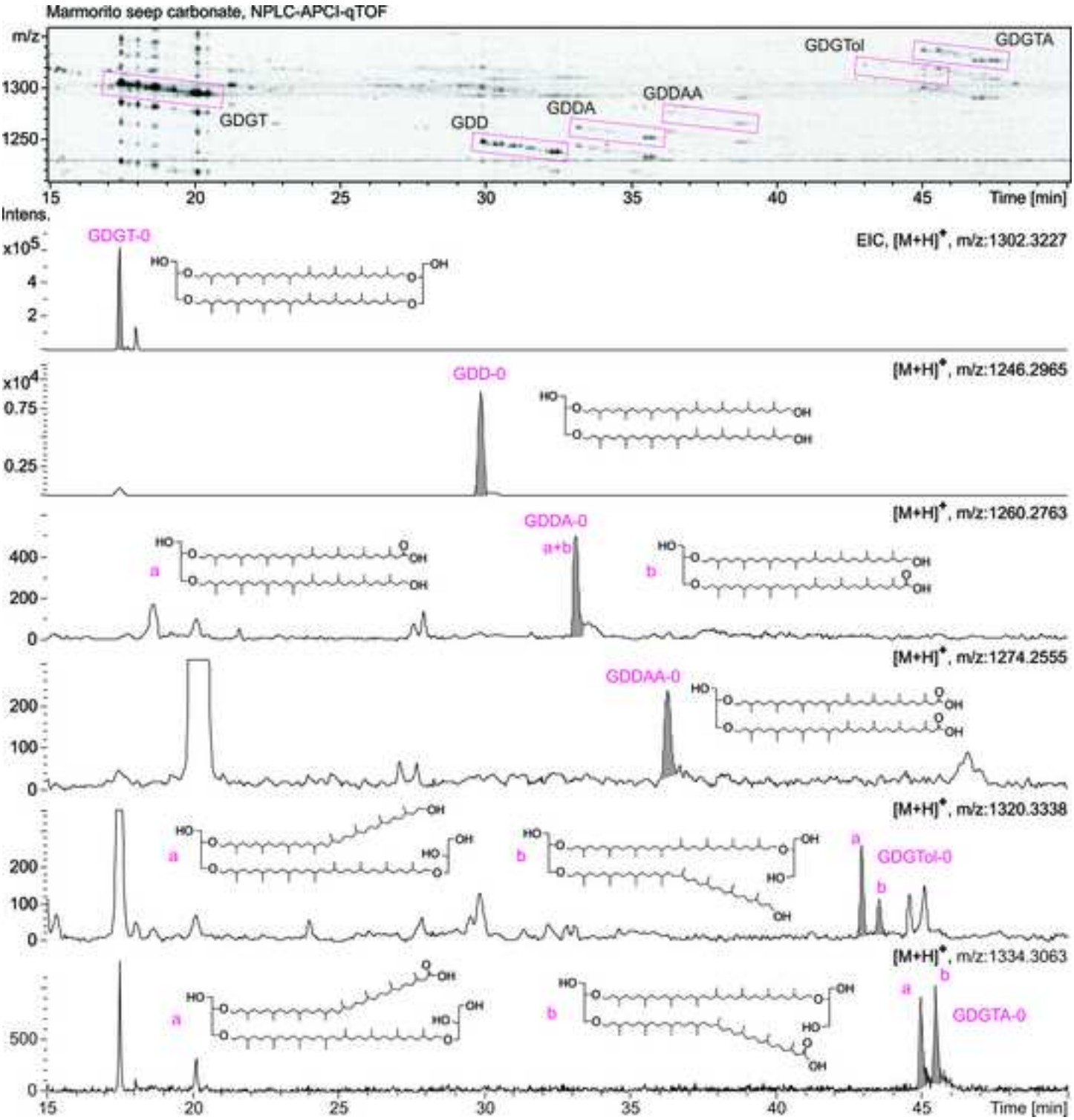

Figure

Click here to download high resolution image

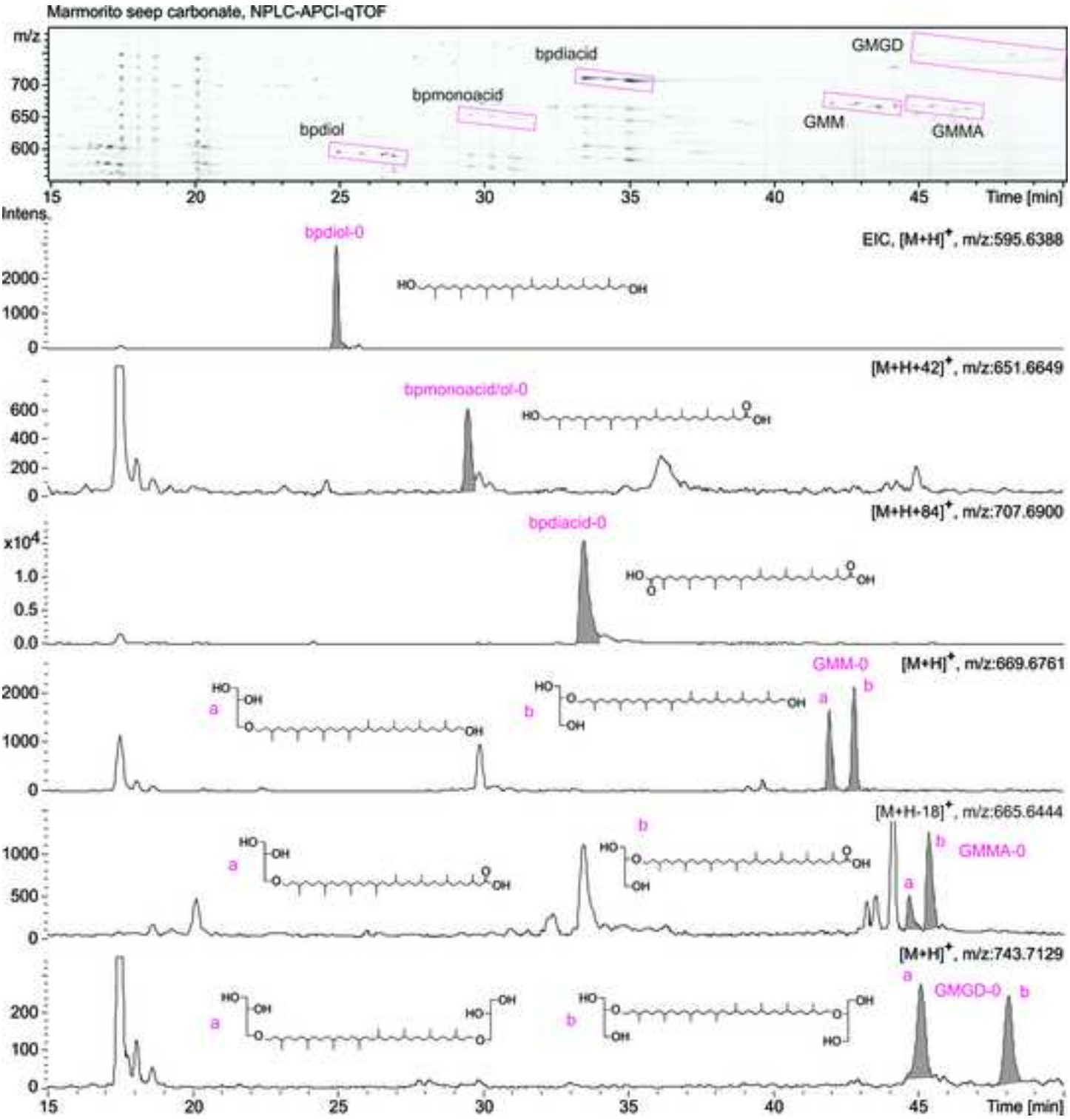

Figure

Click here to download high resolution image

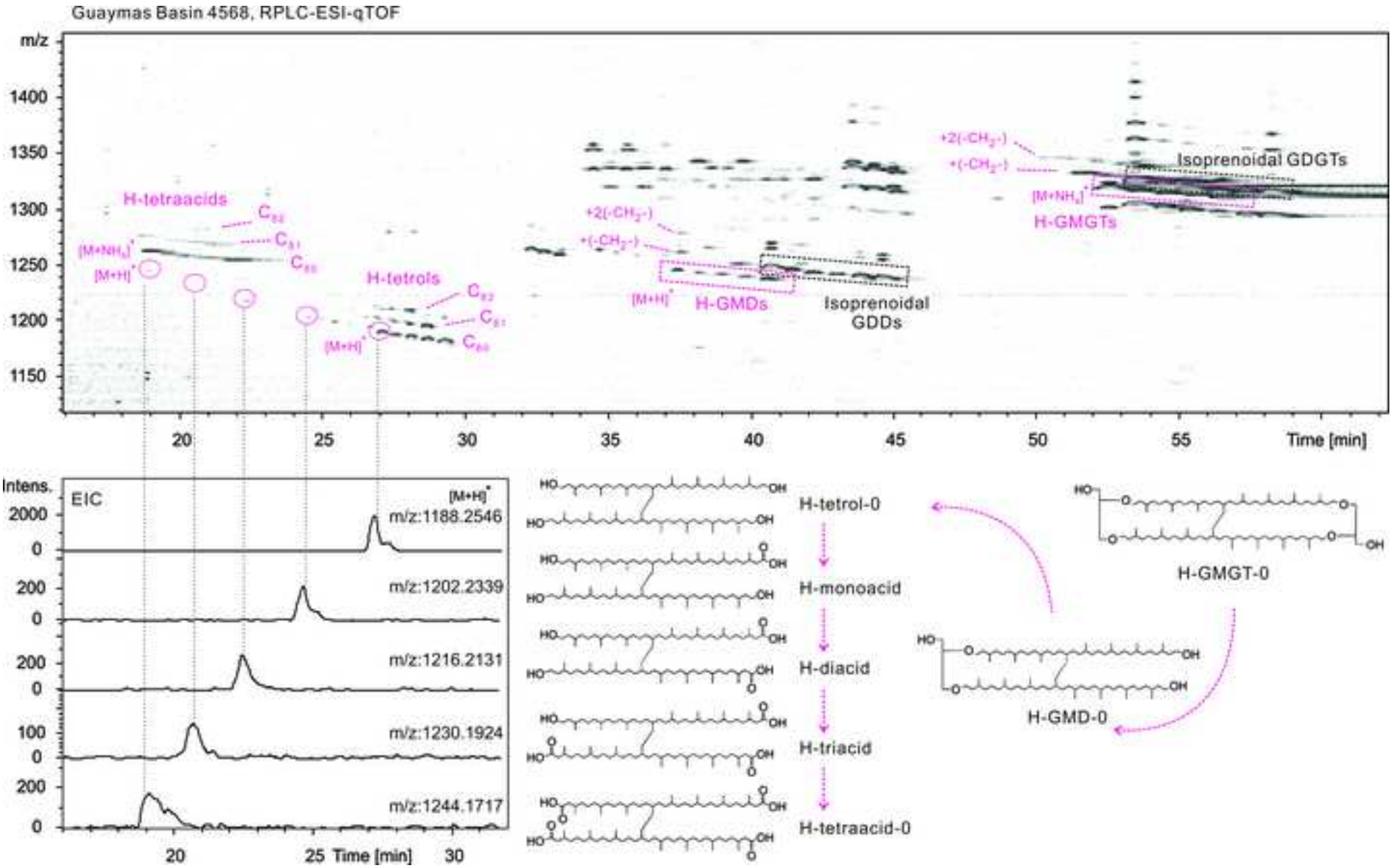

Figure
Click here to download high resolution image

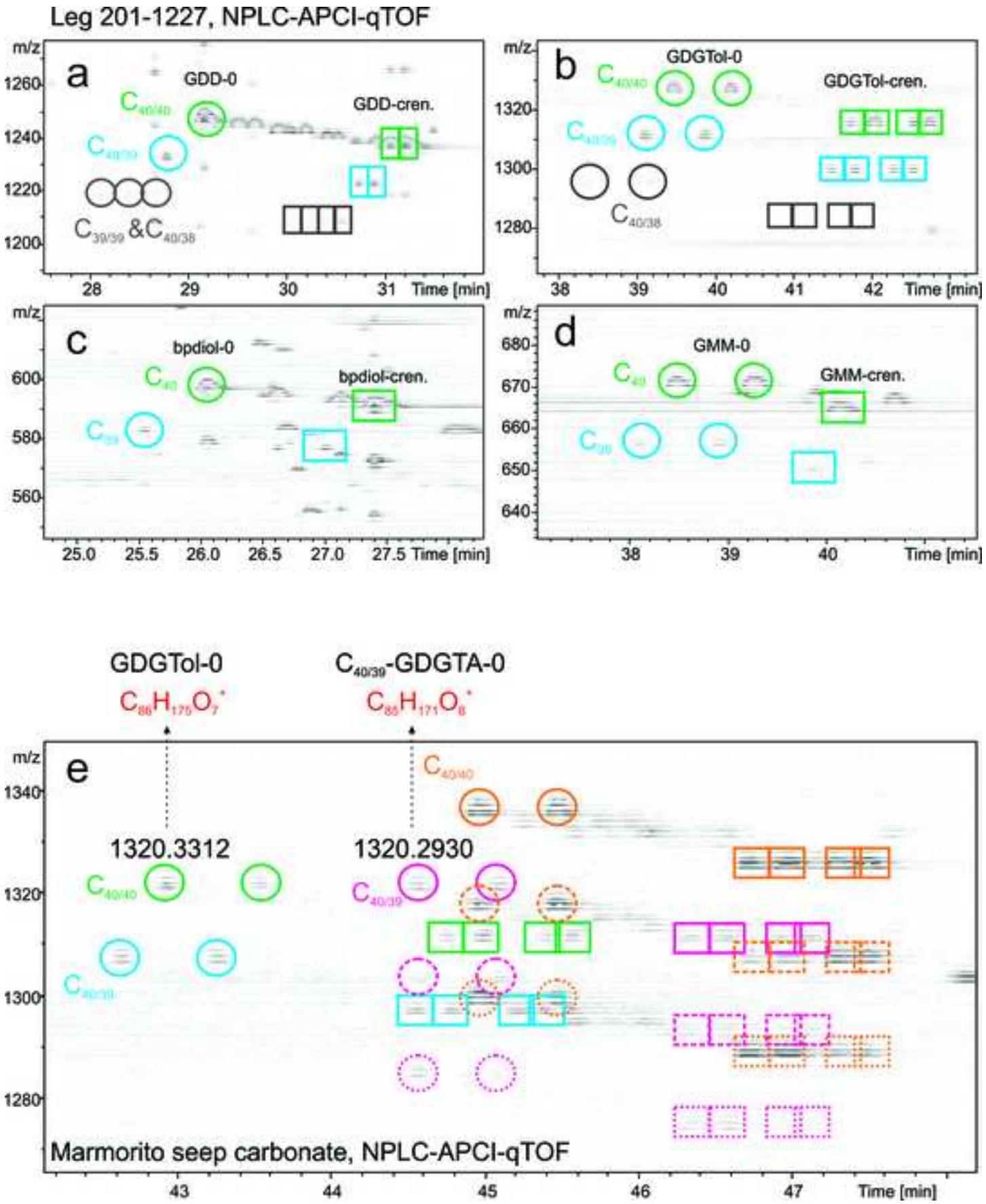

Figure
Click here to download high resolution image

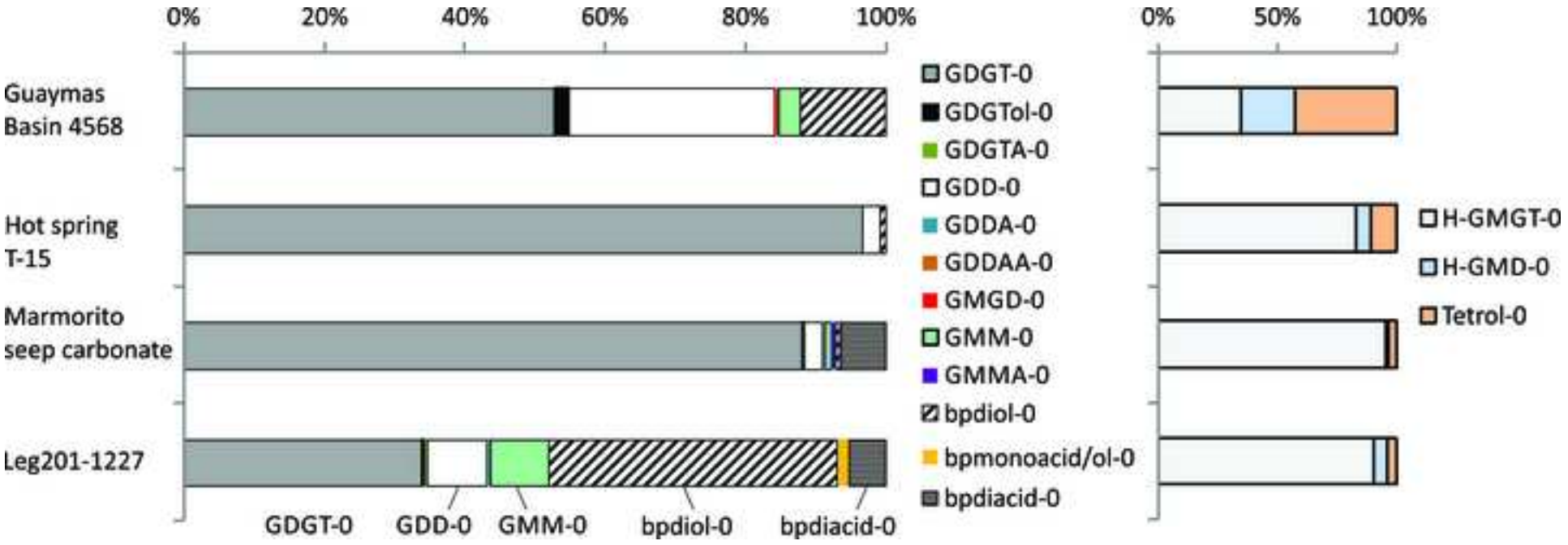

Figure
Click here to download high resolution image

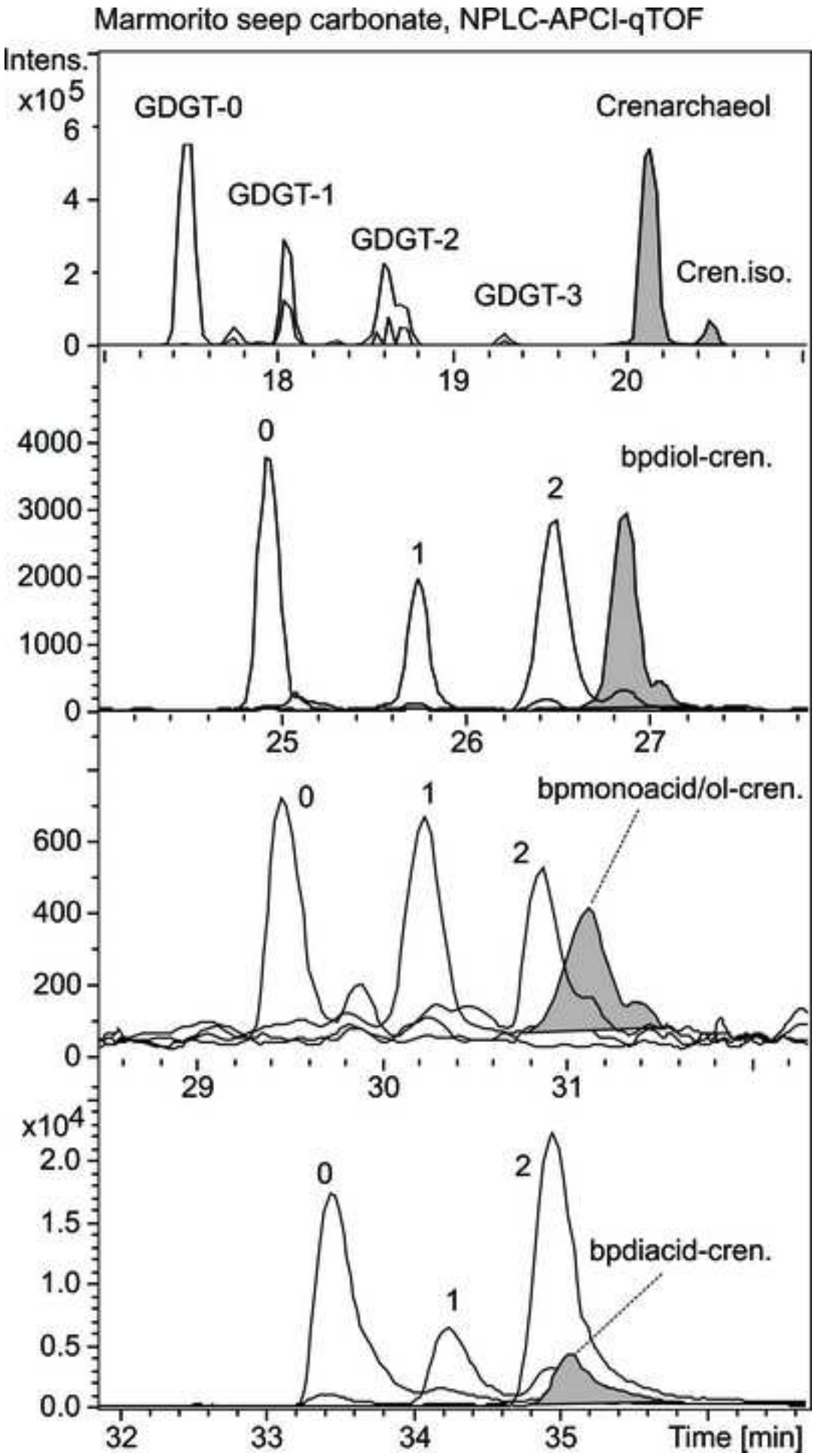

Figure
Click here to download high resolution image

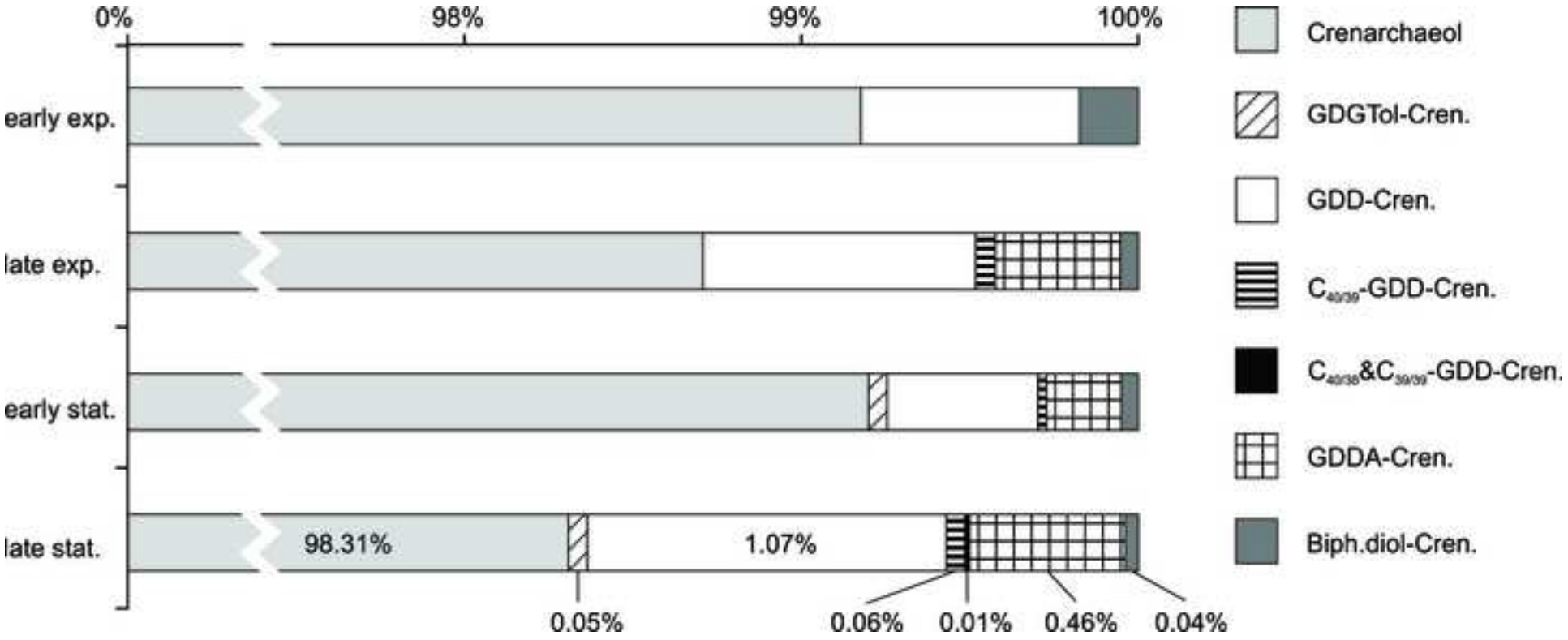

Figure

Click here to download high resolution image

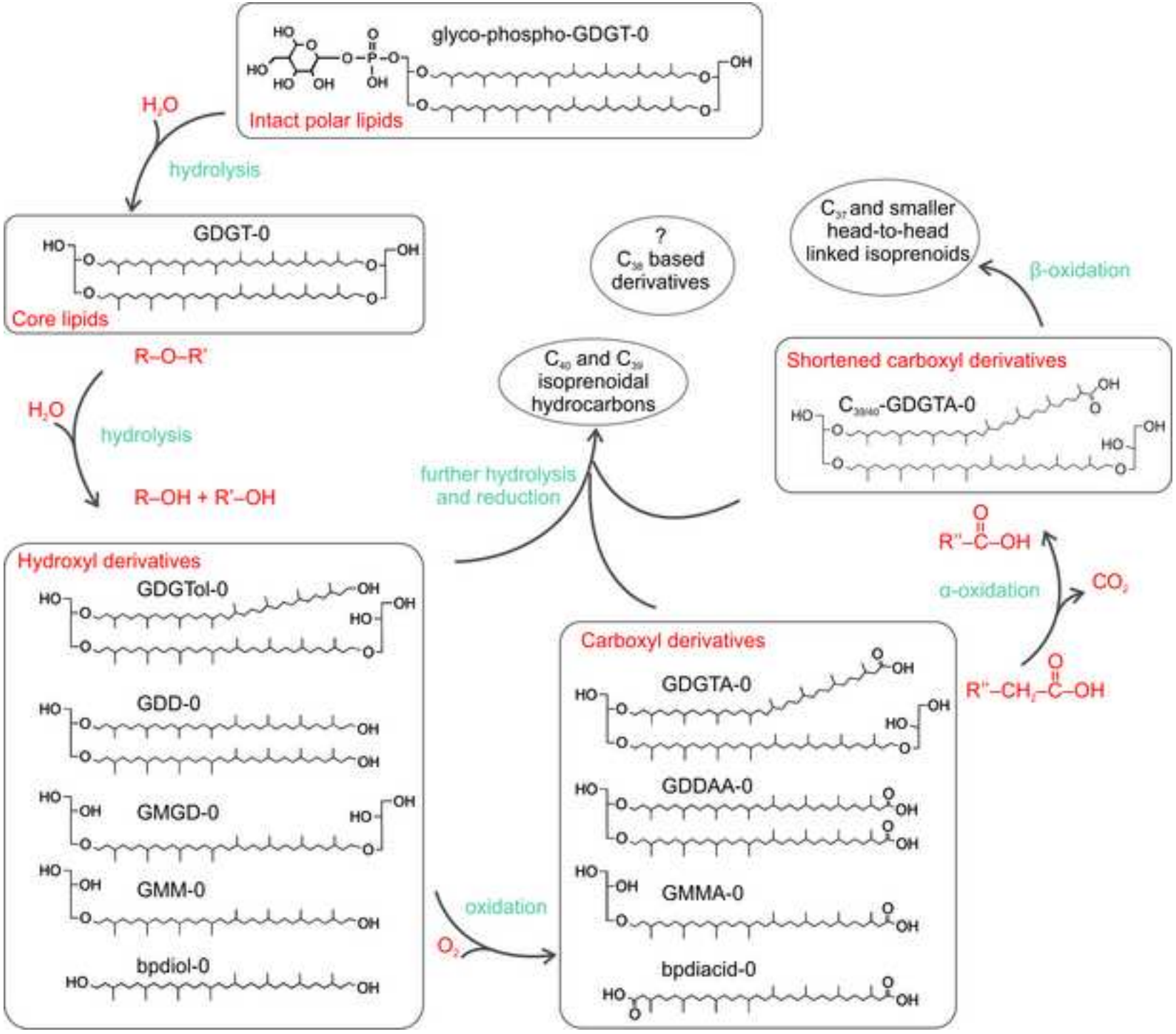

Figure

Click here to download high resolution image

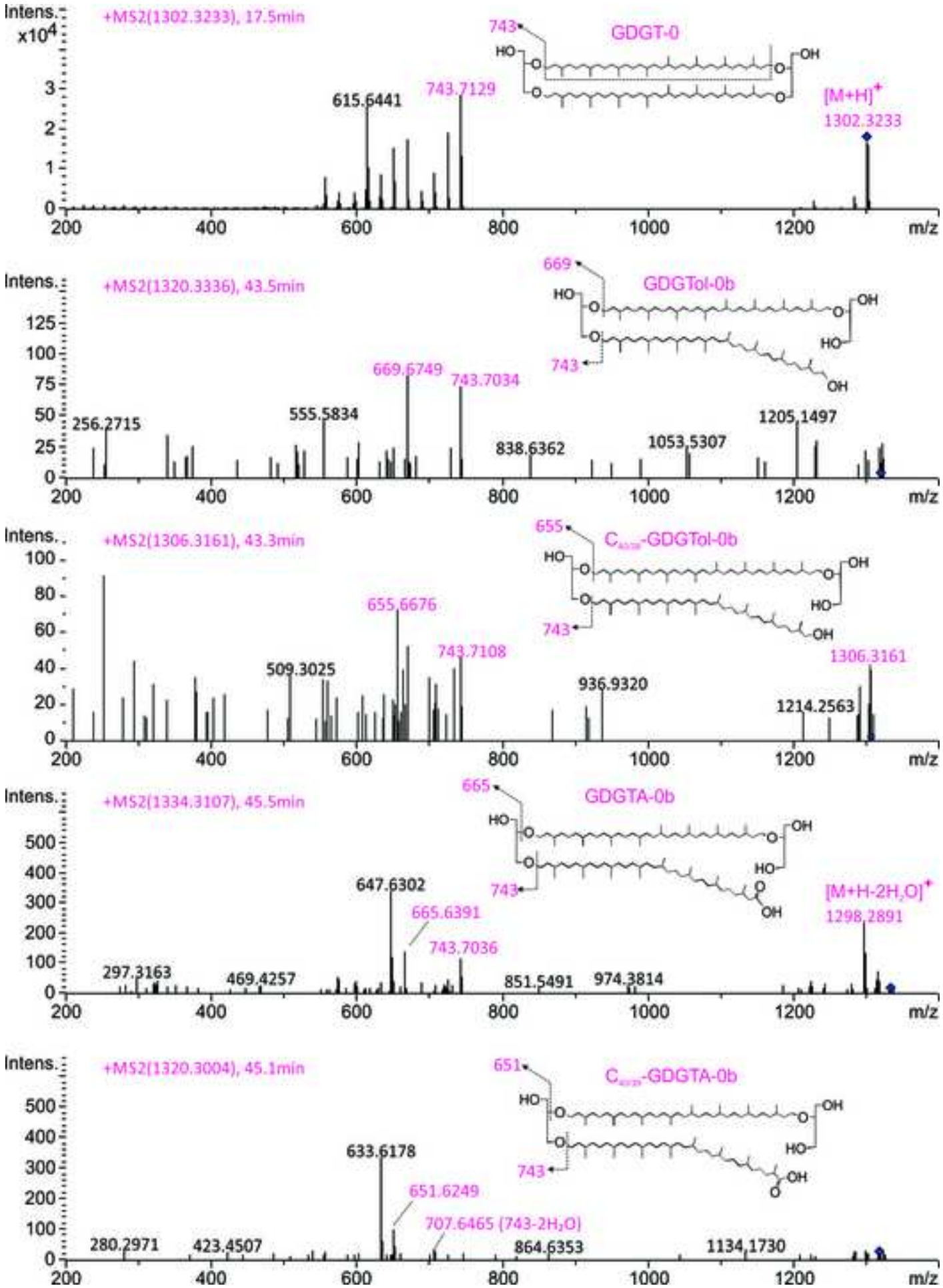

Figure

Click here to download high resolution image

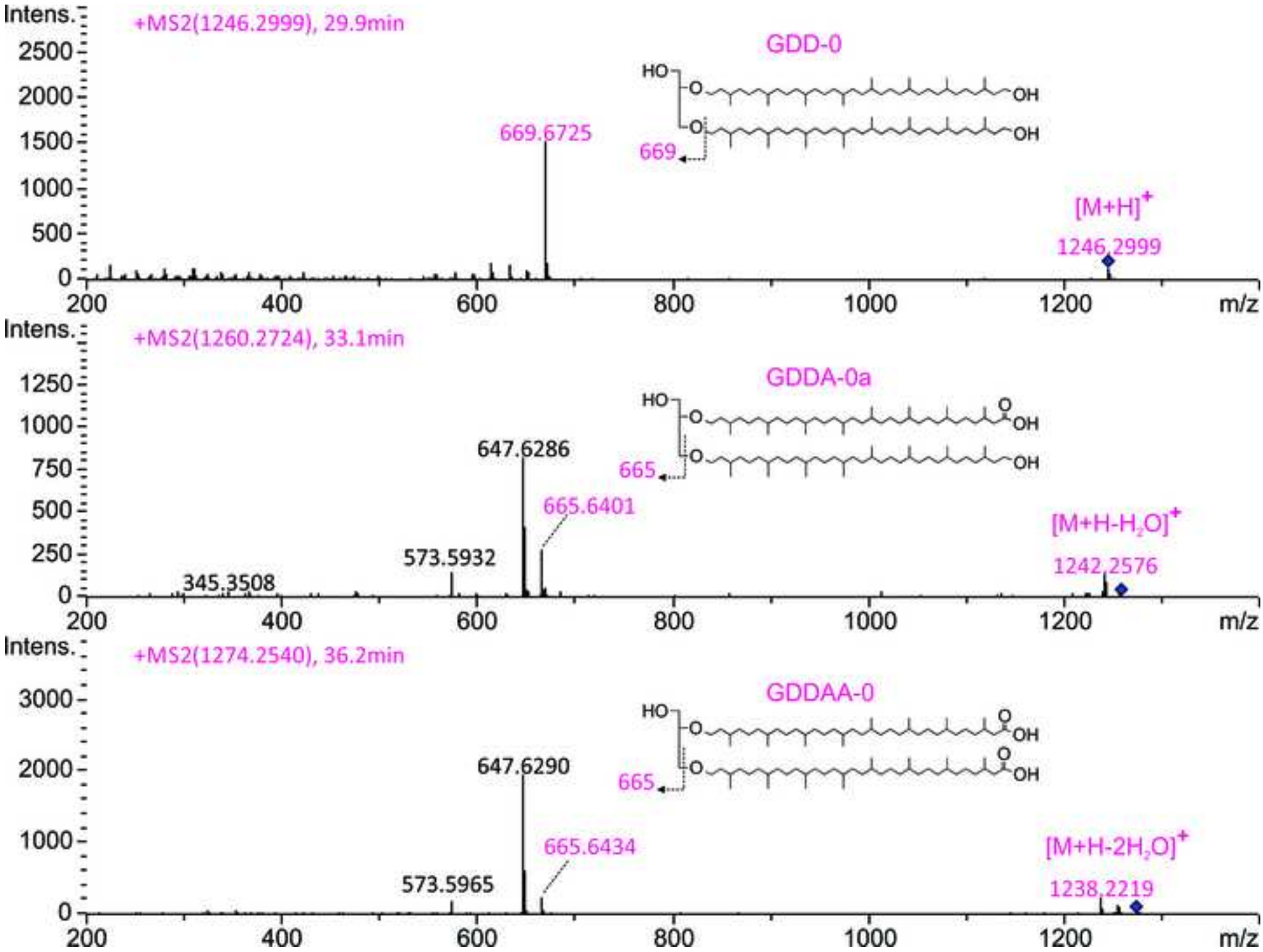

Figure

Click here to download high resolution image

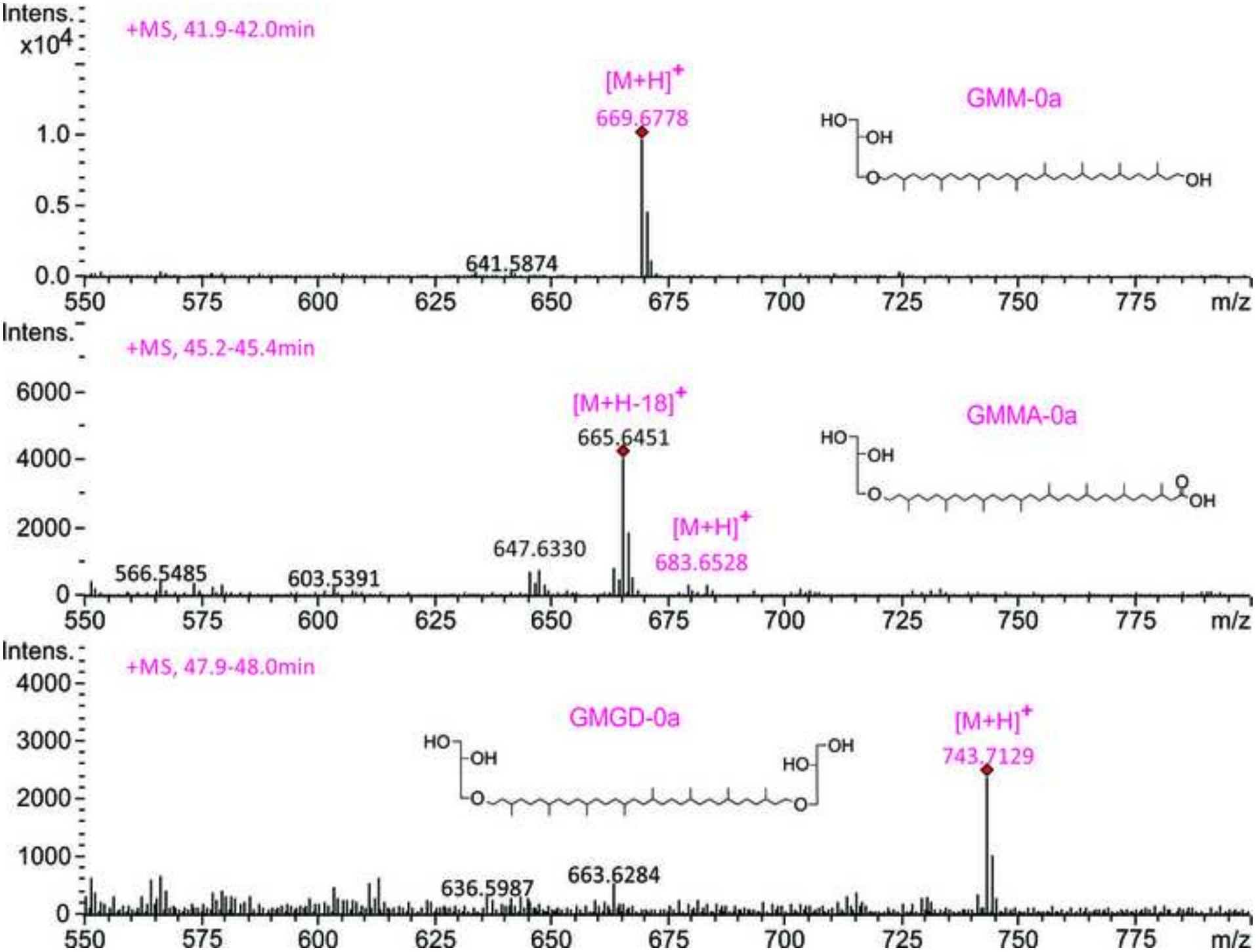

Figure

Click here to download high resolution image

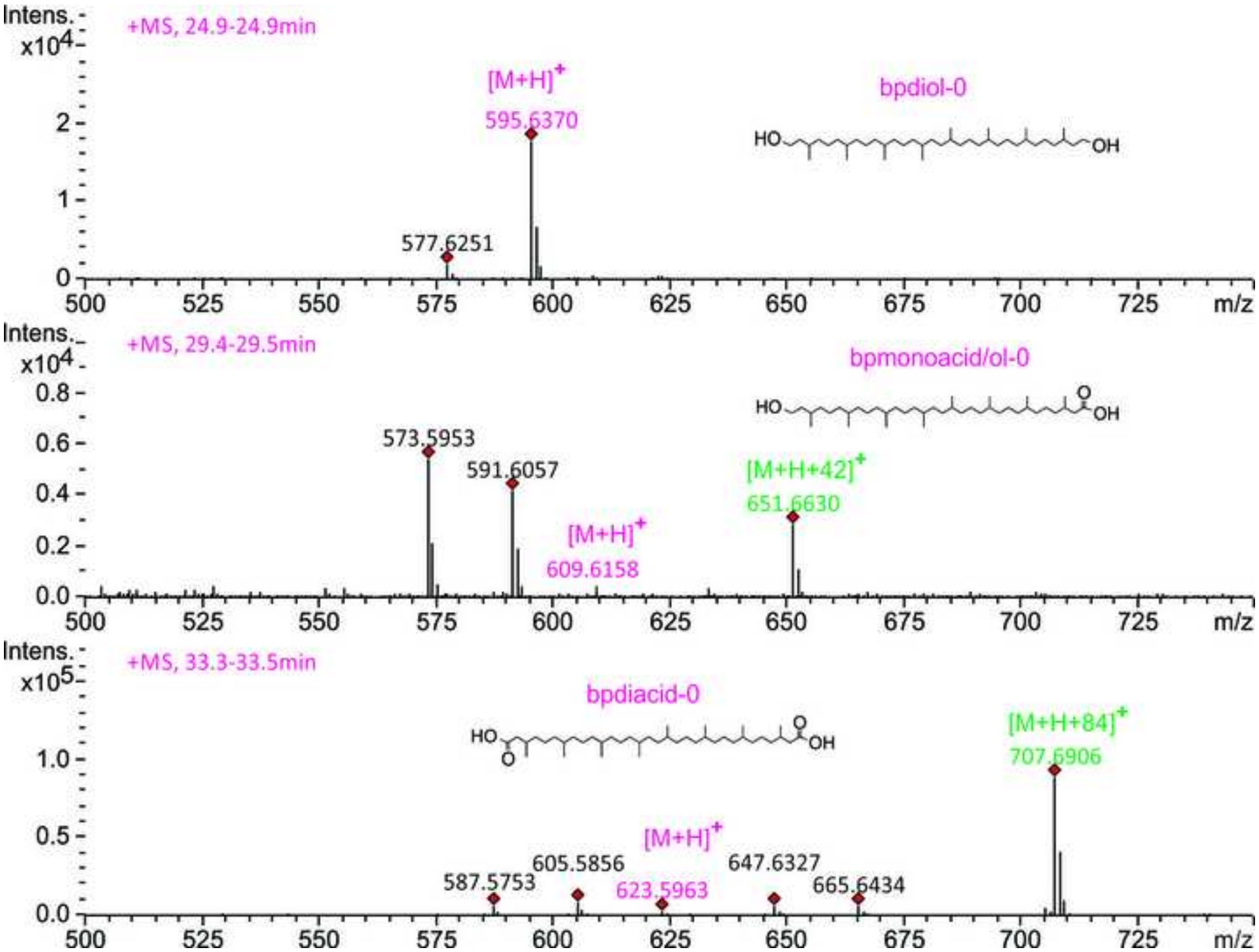

Figure

Click here to download high resolution image

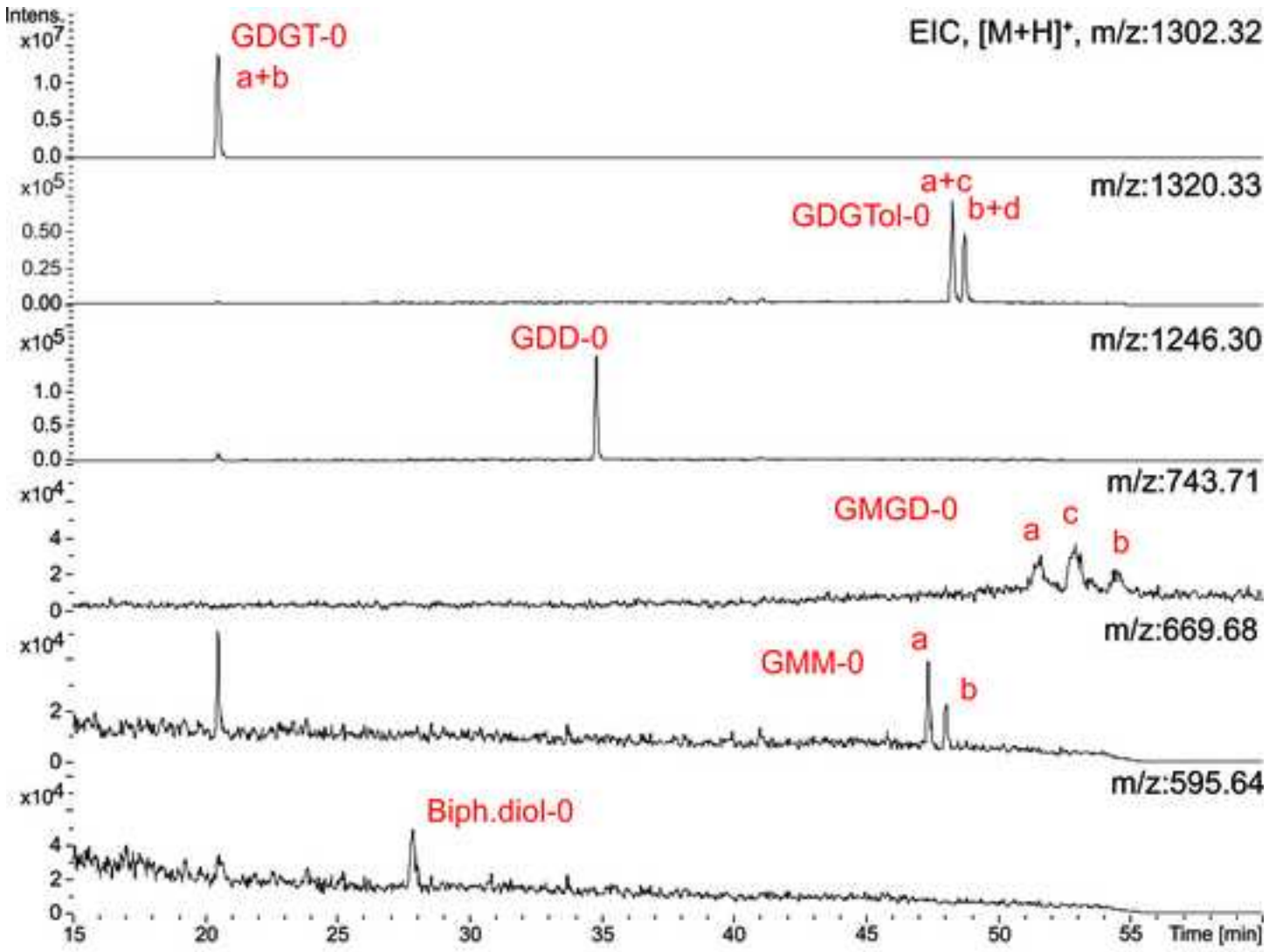

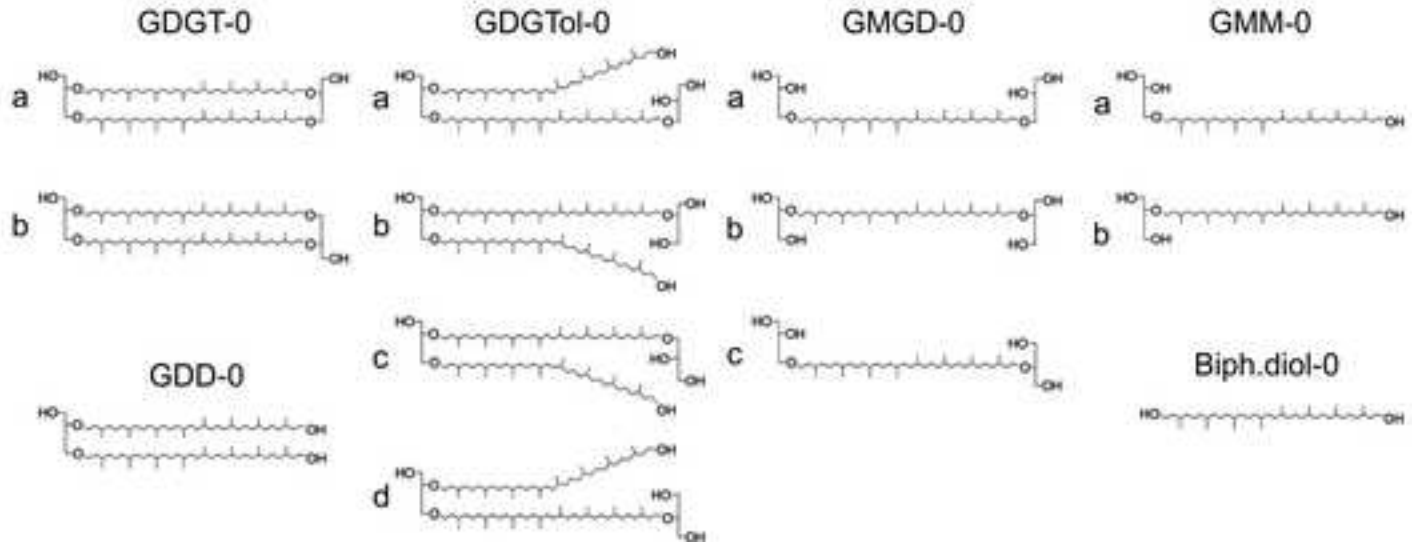

Figure

Click here to download high resolution image

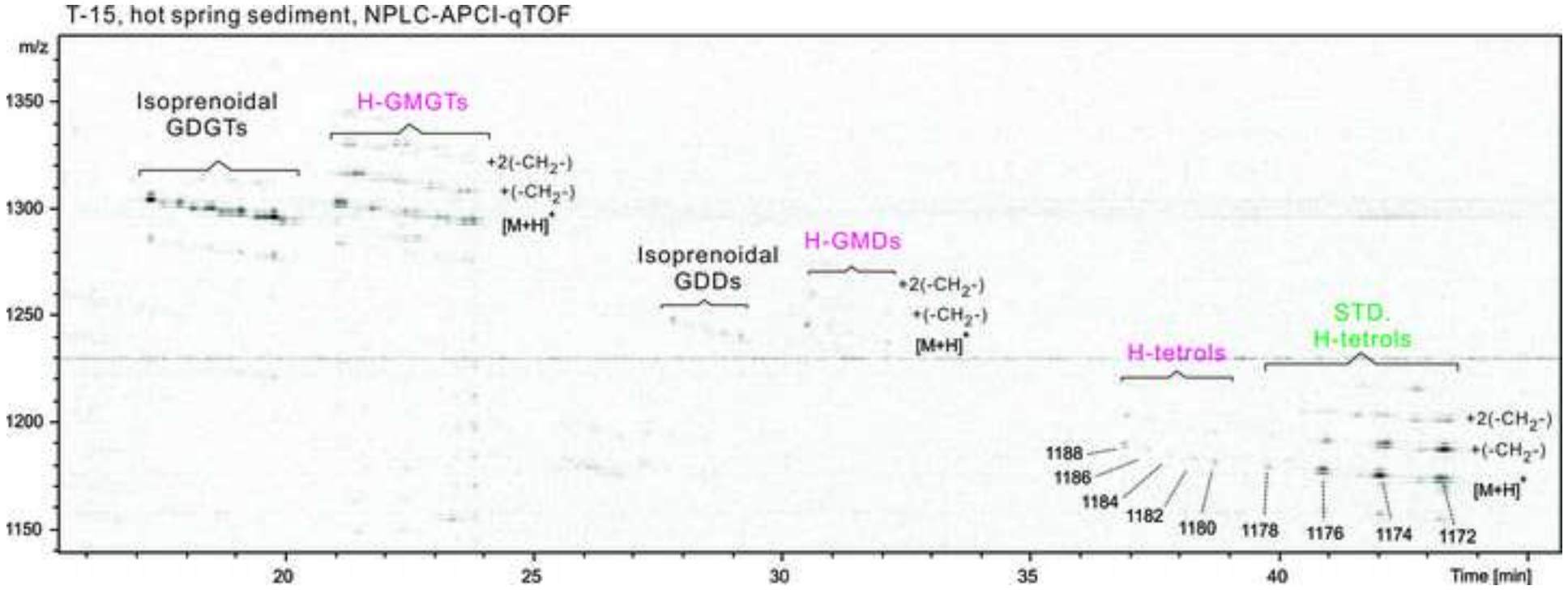

Figure
Click here to download high resolution image

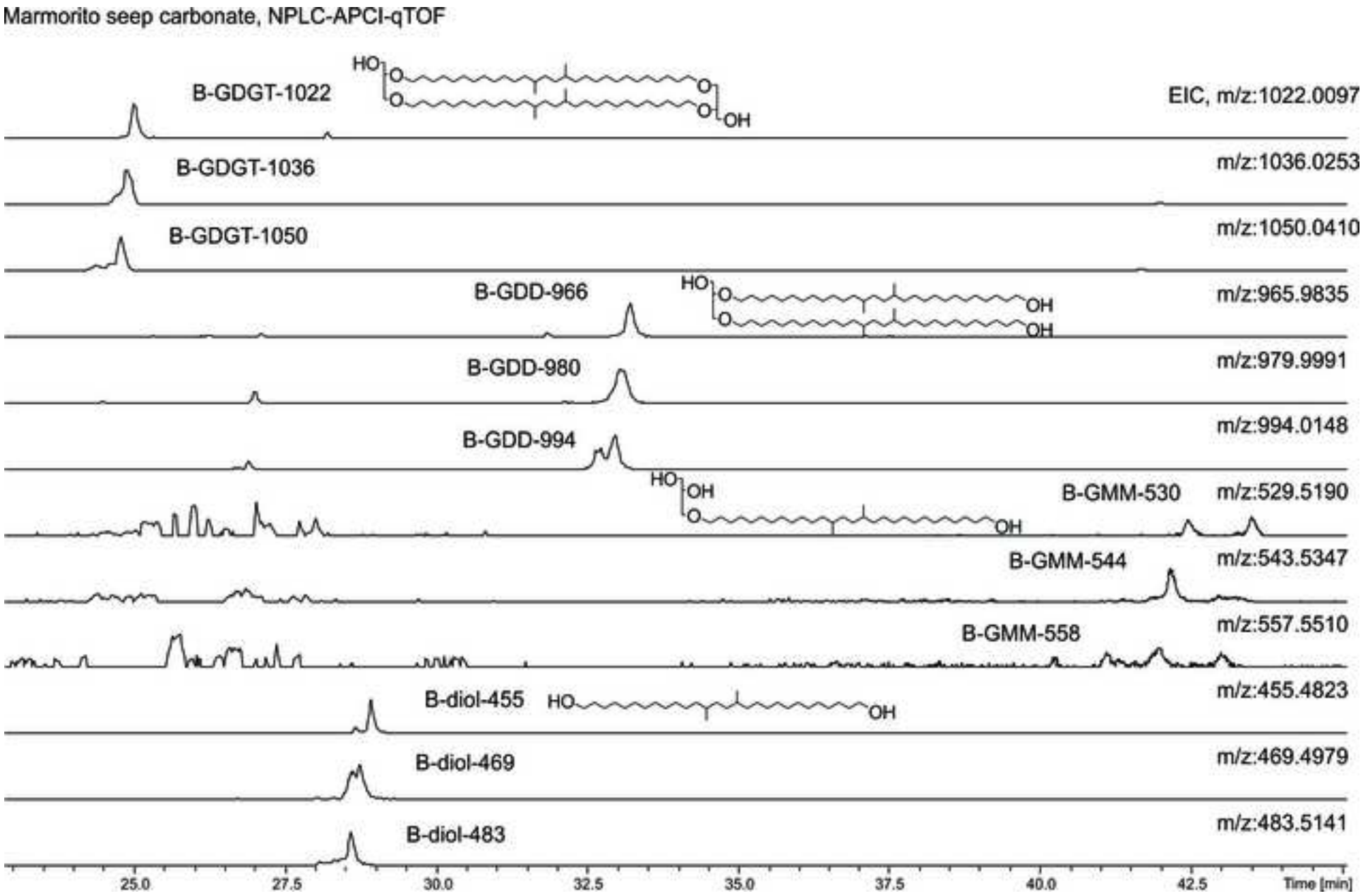

Figure
Click here to download high resolution image